$MoS_2/Cd_{0.90}Zn_{0.10}Te_{0.93}Se_{0.07}$ vdW INTERACTED HETEROSTRUCTURE FOR PHOTOVOLTAIC APPLICATIONS WITH ENHANCED ABSORPTION IN VISIBLE REGION

A dissertation submitted in the partial fulfilment of the requirement for the award of the degree of

Master of Technology

In

VLSI and Embedded Systems

Submitted by:

PRATEEK TOMAR

2K18/VLS/11

Under the supervision of

Mr. Anurag Chauhan

Assistant professor

ELECTRONICS & COMMUNICATION ENGINEERING

DELHI TECHNOLOGICAL UNIVERSITY

(Formerly Delhi College of Engineering)

Bawana Road, Delhi- 110042

2018-2020

CANDIDATE'S DECLARATION

I **Prateek Tomar**, Roll no. **2k18/vls/11** student of **M.TECH** with specialization in **"Vlsi and embedded systems"** hereby declare that the project dissertation titled **"MoS_2/$Cd_{0.90}Zn_{0.10}Te_{0.93}Se_{0.07}$ vdW interacted heterostructure for photovoltaic applications with enhanced absorption in the visible region"** which is submitted by me to the Department of **Electronics and Communication Engineering**, **Delhi Technological University, Delhi** in the fulfillment of the requirement of the award of the degree **of Master of Technology** is original and not copied from any source without proper citation. This work has not previously formed the basis of the award of any Degree, Diploma Associateship, Fellowship or other similar title or recognition.

prateek tomar

Place: Delhi **PRATEEK TOMAR**

Date: 31-oct-2020 **2K18/VLS/11**

CERTIFICATE

I hereby certify that the project dissertation titled **"$MoS_2/Cd_{0.90}Zn_{0.10}Te_{0.93}Se_{0.07}$ vdW interacted heterostructure for photovoltaic applications with enhanced absorption in visible region"** which is submitted by **Prateek Tomar**, Roll No. **2k18/vls/11** in the fulfillment of the requirement of the award of the degree of **Master of Technology** with specialization in **"VLSI and Embedded systems"** is a record of project work carried out by the student under my supervision. To the best of my knowledge this work has not been submitted in part or full for any Degree, Diploma Associateship to this university or elsewhere.

Place: Delhi **MR. ANURAG CHAUHAN**

Date: 31-oct-2020 **SUPERVISOR**

ACKNOWLEDGEMENT

It is a matter of distinct pleasure for me to express a deep sense of gratitude and indebtedness to my learned supervisor **Mr. Anurag Chauhan,** Assistant professor in the Department of Electronics and Communication Engineering, Delhi Technological University, Delhi, for his invaluable expert guidance and patient review. His continuous inspiration has made me complete this major dissertation.

I am also thankful to my friends and classmates for their unconditional support and motivation during the project.

PRATEEK TOMAR

2K18/VLS/11

ABSTRACT

In recent years two-dimensional materials such as hexagonal boron nitride (h-Bn), transition metal dichalcogenides (TMDCs), and graphene have arisen as a very unique class of materials which can be a better alternative of traditionally semiconductors like Ge, Si, and GaAs with unique properties such thickness-dependent tunable bandgap. Their electronic and optical properties are of great importance for a variety of applications in optoelectronics as light emitters, detectors, and photovoltaic and photo electrochemical energy conversion devices. This work focuses on the vdW interacted heterostructure of MoS_2 and $Cd_{0.90}Zn_{0.10}Te_{0.93}Se_{0.07}$, the properties of monolayer MoS_2 are investigated as well as the properties of $Cd_{0.90}Zn_{0.10}Te_{0.93}Se_{0.07}$ to provide an understanding of their significant difference. A detailed investigation of the electrical and optical properties of the heterostructure of the monolayer ($Cd_{0.90}Zn_{0.10}Te_{0.93}Se_{0.07}$) and monolayer MoS_2 is done by first-principles calculations. For calculating the electronic as well as optical properties of MoS_2/ $Cd_{0.90}Zn_{0.10}Te_{0.93}Se_{0.07}$ heterostructure, density functional theory (DFT) based simulations is performed on Atomistic Tool Kit (ATK). Hence the heterostructure of cadmium zinc telluride selenium ($Cd_{0.90}Zn_{0.10}Te_{0.93}Se_{0.07}$) and monolayer MoS_2 with Van der Waals (VdW) interaction is suggested for tuning the optical absorption in the visible region. First-principles study on the structure-property relationships in monolayer MoS2 and vertically stacked membrane of $Cd_{0.90}Zn_{0.10}Te_{0.93}Se_{0.07}$ interacted with VdW forces of attraction enables the possibility to exfoliate and reassemble different 2D material which holds the properties of the individual material. The results show the absorption in MoS_2/ $Cd_{0.90}Zn_{0.10}Te_{0.93}Se_{0.07}$ heterostructure shifted to entirely in the visible region, range of wavelength 400 nm 550 nm with having negligible absorption in UV and infrared region that is an indication that devices made from this material will be of high efficiency with less heating possibilities and it is also found monolayer MoS_2 has absorption in ~300 nm ~360 nm of wavelength and for $Cd_{0.90}Zn_{0.10}Te_{0.93}Se_{0.07}$ absorption is high in the range of ~130 nm ~250 nm hence heterostructure resulted into direct bandgap structure that finds the number of application in optoelectronics.

TABLE OF CONTENTS

LIST OF FIGURES

LIST OF TABLES

List of symbols

χ	Extinction coefficient
$\hbar$	Planck constant
η	Refractive index
σ	Optical conductivity
α	Polarizability
ε_r	Relative dielectric constant
ε_0	Dielectric constant
ω	Photon frequency

CHAPTER 1

INTRODUCTION

1.1 Overview

Electronics is undergoing a significant transformation because the doubling of silicon transistors no longer results in advantages of energy efficiency, stimulating research into nanotechnologies beyond silicon. Researchers have been studying and working with nanoparticles for decades and they were not able to see the structure of nanoparticles. With the advancements of microscopes in recent decades, researchers got the ability to see these Nano-sized structures which are as small as atoms and this had opened up a world of possibilities in a variety of industries and research ventures. The National Science Foundation (NSF) states nanotechnology as a task at a 1-100 nm length scale to fabricate devices, structures that have remarkable properties because of their nano-size structures.

Nano-materials are a miniaturization of materials producing devices or machines on a molecular level, requiring the engineering of materials on an atomic scale, where around two-tenths of a nanometer is called nanotechnology. The use of nanomaterial is also having lot of scope in optoelectronics and photonics research in the carbon nanomaterial such as graphene and CNT, as well as 2D layer materials such as TMDs have opened the wide scope of nanomaterial towards electronics and optoelectronics devices.

1.1.1 Nano Electronics -Nanotechnology in Electronics

Nanoelectronics is characterized as nanotechnology that allows the integration of pure electronic devices, electronic chips and circuits. Digital systems are mixed with analog ones. This form of technology fusion can be defined as the 'More than Moore' creation domain. Nanoscale measurements of nanoelectronics components for giga-scale complexity systems calculated on a chip or box. This scaling function and the path to giga-scale systems can be defined as the 'More Moore' development domain.

1.1.2 Capabilities of Nano Electronic Components

Nanoelectronics gives some answers for how we can increase the capabilities of electronics components while we reduce their size, risk factor, and power consumption for a normal size the power of the device is enough to handily overcome any friction but if we scale its length by a factor of 1000 decreases is power consumption by factor 1000^2 proportionally it is 1000 times less power per unit then the original. Nanotechnology is dedicated to making computer processors more effective than traditional semiconductor manufacturing methods, and field effect transistors have also been manufactured using both carbon nanotubes and heterostructured nanowires.

1.1.3 Semiconductor with Hetero-junctions

Semiconductor nanowires have potentials for optoelectronics devices such as hetero-structures, LEDs, photodetectors, solar cells, quantum devices, memory storage devices, and flexible displays, a device based on photo conduction is shown in Fig.1.1 Low energy consumption displays are now fabricated using CNTs such Nanostructured and are highly conductive with a small diameter can be used as field emitters with high efficiency moreover devices fabricated with hetero-junctions promises the higher absorption rate with tunable optical and electrical conductivity at the same time.

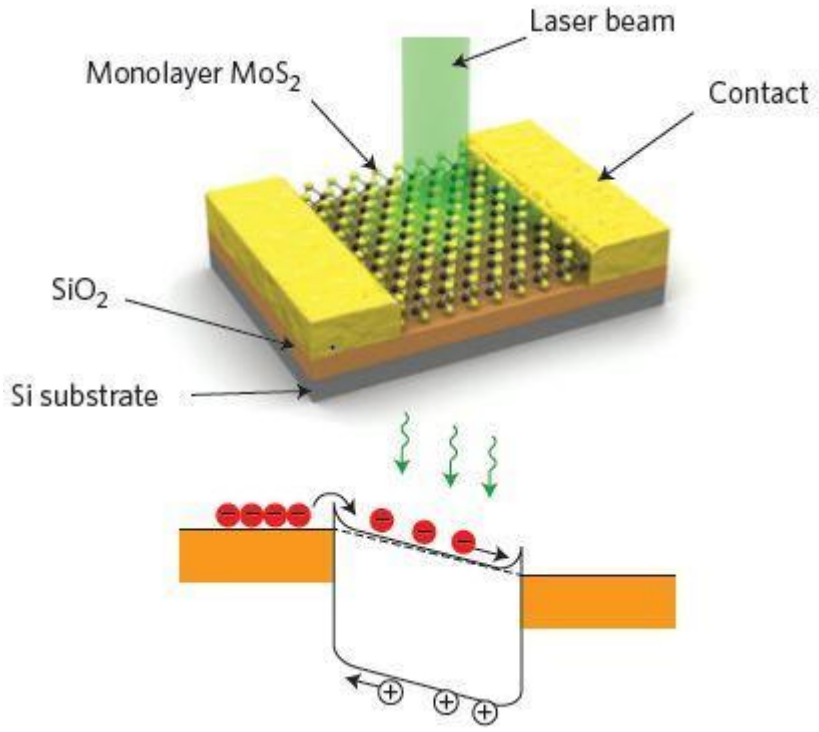

Fig .1.1 Device based on photoconduction [15]

1.2 Introduction to TMDs and heterostructures

In the past few decades, 2D materials have gotten decent attention in the field of Nanoelectronics due to their ultimate dimension and unique physical properties. Graphene is a single layer of carbon atoms in honeycomb structure lattice. The Discovery of graphene started the journey of 2D materials and most of them having potential for nanophotonics and spintronics applications make them suitable for atomically thin structures with novel properties hence graphene has attracted much interest due to the immense range of desirable properties that it possesses, like high electron mobility, high strength, and very high thermal conductivity in spite of having remarkable properties graphene cannot be a perfect candidate for all short of electronics problems and that problem is its IDEAL bandgap.

Hence this limitation of graphene makes it unsuitable for most of the electronics applications in transistors and optoelectronics hence this bandgap problem led the researchers to think beyond graphene that led them to another class of 2D nanomaterial called TMDs. Moreover, the structure of these 2D materials is different from graphene in that it consists of the transition layer of metal atoms which are sandwiched between two layers and which are bound with tight covalent bonds.

1.2.1 TMDS over graphene

Moreover, graphene has proved itself a promising material in the various fields of modern electronics such as wearable and superfast electronics, medicine and ultra-sensitive sensors [2]. Graphene is having some outstanding properties if we compare to the commonly used Ge and Si semiconductor its mobility is 100 times faster than Si, electrical conductivity is 15 times better than silver and it absorbs 10% of its incident radiation moreover graphene defect-free monolayer is the strongest material ever tested [2][6].

Now we talk about TMDs over the last few years, TMDs had proved themselves promising candidates that could replace graphene in the near future. Graphene is semi-metal this means that with the application of small voltage electrons can move fast that can generate desirable ampere of current which means devices made of graphene are very difficult to turn off, unlike monolayer MoS_2 has a sufficient energy gap that results large on/off current ratio. So we are not able to use graphene in FET transistors despite this researchers

also reported that transistors fabricated with MoS_2 consume 10000 times less energy than traditional Si transistors hence MoS_2 atomic layers can be used as a channel or gate dielectric for fabricating thin-film FETs for electronics and optoelectronics applications[6].

1.2.2 TMDs and their structures

Transition Metal dichalcogenides (TMD) are the semiconductor of type MX_2. Where M are transition metals, and where X are chalcogens. Many different TMDs are feasible due to the different metal transition and chalcogen permutations that can be produced. In TMD structures M are transition metals can Molybdenum (Mo-42**)** and tungsten (W-74) and can be any of these elements sulfur(S-16), Tellurium (Te-52) and Selenium (se-34).

Since most semiconducting TMDs have a band gap < 2 eV, many monolayer TMDs also have a direct band gap, favorable electronic and mechanical properties that allow their use in the field of optoelectronics, which are excellent candidates for future electronic devices.

For future electronic devices, the great promise of 2D materials, especially TMDs, needs a detailed study of their electronic properties for transportation. The semiconductive structure of MoS_2, which belongs to the family of transition metal dichalcogenides TMDs, has a considerable band-gap. The form and value of MoS_2 band gap can be changed by increasing the number of MoS_2 layers, with a 1.2 eV indirect band gap (multilayers) and a 1.8 eV direct band gap if it is limited to a monolayer. Hence these materials show band gap near infrared region of the electromagnetic spectrum thus it had opened applications of these materials in photonics and optoelectronics.

1.3 Introduction to MoS_2

2D transition metal dichalcogenides (2D-TMDs) [5, 6, 7, and 8] have emerged as promising options in optoelectronic devices owing to their novel properties, such as excellent mechanical and thermal stability. Usually, TMD member molybdenum disulfide (MoS_2) has good light matter interactions and excellent absorption potential in the visible light area range, creating remarkable photovoltaic applications. Besides this, MoS_2 shows considerable carrier mobility of ~200 $cm^2\,V^{-1}\,s^{-1}$ for monolayer and ~500 $cm^2\,V^{-1}\,s^{-1}$ for multi-layer. The weak interlayer vdW interactions, meanwhile, allow the separation of wide area and uniform MoS_2 atomic layers, and the removal of weak bonds is

advantageous for heterostructures to form. Fig. 3.1 and Fig. 3.2 shows coplanar and hybrid van der Waals contacts to 2D semiconductors.

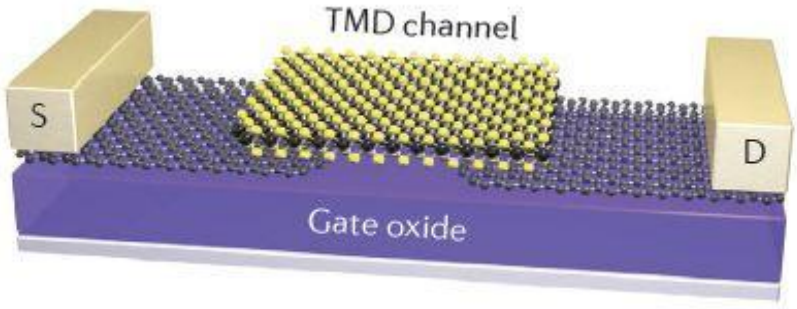

Fig. 1.2 Schematic diagram of coplanar van der Waals contacts 2D semiconductor [18]

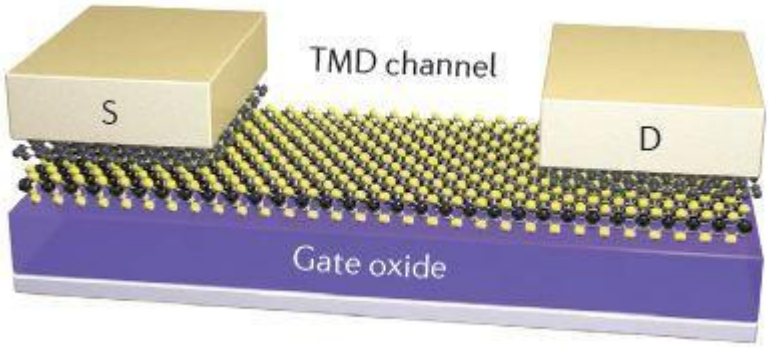

Fig. 1.3 Schematic diagram of hybrid van der Waals contacts 2D semiconductors [18]

TMDs are therefore commonly used as a modern channel material with improved application geometry for atomically thin transistors.

The successful growth of monolayer and few-layer MoS_2 has generally triggered the development of electronic nanodevices based on MoS_2. Light absorption in a monolayer MoS_2 [8] is produced by dipole transitions between localized *d* orbitals, which yields an absorption for a single layer MoS_2 flake at the level of 2–5% in the visible range.

1.4 Introduction to Cadmium Zinc telluride

This wide gap semiconductor material had attracted a number of researchers over the last decade which increased the interest as X-ray and gamma-ray detectors. Compared to this CdTeZn material, spectrometers fabricated with Si and Ge has extremely low detection efficiencies. CdTeZn shows good room temperature performance hence it is the best option for the development of a compact reliable detection system.

Traditional semiconductors used for radiation detectors are Si and Ge, providing successful results in a wide group of applications. The production of detectors focused on compound semiconductors has been boosted by the emerging field of applications. The probability of increasing materials with a wide variety of physical properties (band distance, atomic number) is a great advantage of compound semiconductors, making them ideal for almost any application. The interest in radiation detectors operating at room temperature has contributed to the creation of compound semiconductors relative to Si and Ge with large band gaps.

Table 1.1 Physical properties of the most important semiconductor compounds commonly used for the detection of radiation [29].

Substance	Si	Ge	GaAs	CdTe	$Cd_{0.9}Zn_{0.1}Te$
Atomic number	14	32	31,33	48,52	48,30,52
Pair creation energy (eV)	3.42	2.96	4.2	4.43	4.6
Resistivity(Ωcm)	10^4	50	10^7	10^9	10^9
Density (g/cm^3)	2.33	5.33	5.33	6.20	5.78
Crystal structure	Cubic	Cubic	Cubic(ZB)	Cubic(ZB)	Cubic(ZB)
Growth method	C	C	CVD	THE	THM
$\mu_e\tau_e$	>1	>1	10^{-5}	10^{-4}	10^5
Bandgap (eV)	1.12	0.67	1.43	1.44	1.57

Common growth methods: **THM = Traveler heater method ,THM=Traveler heatermethod, C = Czochralski, CVD = chemical vapor deposition BM = Bridgman method, VAM = Vertical ampoule method and HPB = high pressure Bridgman**

CdTe and CdZnTe have drawn increasing interest from compound semiconductors in the production of gamma-ray and X-ray detectors [5, 6]. CdTe and CdZnTe detectors maintain high detection reliability, decent room temperature accuracy and are very desirable for X-ray and gamma-ray applications because of the high atomic number and large band gap.

Difficulties in producing detector-grade materials and in creating chemically pure and structurally perfect crystals are the crucial obstacles of CdTe and CdZnTe detectors. Indeed, owing primarily to the limited commercial supply of high-quality crystals, for

many decades, the great potential of such substances has not been explored. With the advent of a few corporations dedicated to the advancement and commercialization of these products, this situation changed drastically during the mid-nineties.

For the manufacture of radiation detectors with indifferent frameworks, the material properties of cadmium zinc telluride ($Cd_{1-x}Zn_xTe$ or CZT) with Zn concentrations in the range x from 0,1 to 0,2 CZT in this composition range are used [13] [14]. Based on the value of x we Change the band gap of this material. However, the disadvantages associated with CZT crystals are few. Firstly, it has comparatively high impurity concentrations and intrinsic defects that cause short lengths of drift. Secondly, the poor mobility of the hole, caused by charge trapping, thus strengthened these defects by applying selenium to the CZT.

1.4.1 Role of Selenium addition in CZTs

As we addressed the broad variety of applications where operability at room temperature, high power efficiency and reliability are needed, but CZT is still difficult to manufacture material because production costs and growth have remained high , causing economic difficulties for suppliers. Due to these 3 main detrimental defects below, CZTs suffer from low yield.

- Compositional Inhomogeneity
- High concentration of Te inclusions/ precipitates
- Strong dislocation wall /sub grain boundary network concentration

A new quaternary material $Cd_{1-x}Zn_xTe_{1-y}Se_y$ (CZTS) was adapted to eliminate the inhomogeneity and sub grain boundaries problems. The addition of selenium has been found to be very successful in the elimination of the development of subgrain boundaries and their networks by reducing Te inclusions accumulation and improving the compositional uniformity in the cultivated ingots.

The substance band-gap was calculated using the analytical formula from the measured composition along the length of the ingot for the $Cd_{1-x}Zn_xTe_{1-y}Se_y$ quaternary compound.

1.5 $MoS_2/Cd_{0.90}Zn_{0.10}Te_{0.93}Se_{0.07}$ heterostructure

Above we have discussed the importance of individual compound MoS_2 and CZT in various applications of optoelectronics, photonics, and electronics hence heterostructures have proved their importance in optoelectronics, traditionally semiconductor heterostructures was fabricated using epitaxial growth technique but now heterostructures can be fabricated by vertically stacking of two-dimensional crystals such as phosphorene and two-dimensional material[5][15][16] these layered materials are held by van der Waals force of attraction hence here we reported vdWheterostructures made of molybdenum disulfide and $Cd_{0.90}Zn_{0.10}Te_{0.93}Se_{0.07}$ monolayers. Since these strong covalent bonds are greater stability of the 2D crystals in the plane and are called heterostructures because these atomically thin layers are not retained by chemical reaction, but constrained by the interaction of weak van der Waals. Hence due to this unique interaction of materials increases the interest for the next generation Nano electronics because it became possible to create high-performance structures.

When these materials are placed on top of each other than their individual properties modifies that gives the idea of making new materials and Nanodevices. These properties can be modified by doing several modifications to the geometry of these materials like optical properties of monolayer MoS_2 can be altered by adding later to this monolayer material resulting make it indirect bandgap material from direct bandgap material. Moreover, all the optical and electrical properties largely depend on the interlayer distance which also defines the stability of the heterostructure, vertically stacking the one material over another this stack represents the assembling of the chosen sequence. Powerful covalent bonds that provide in-plane stabilization and weaker vdW forces are necessary to hold the stack together in 2D formed material such as MoS_2 crystals.

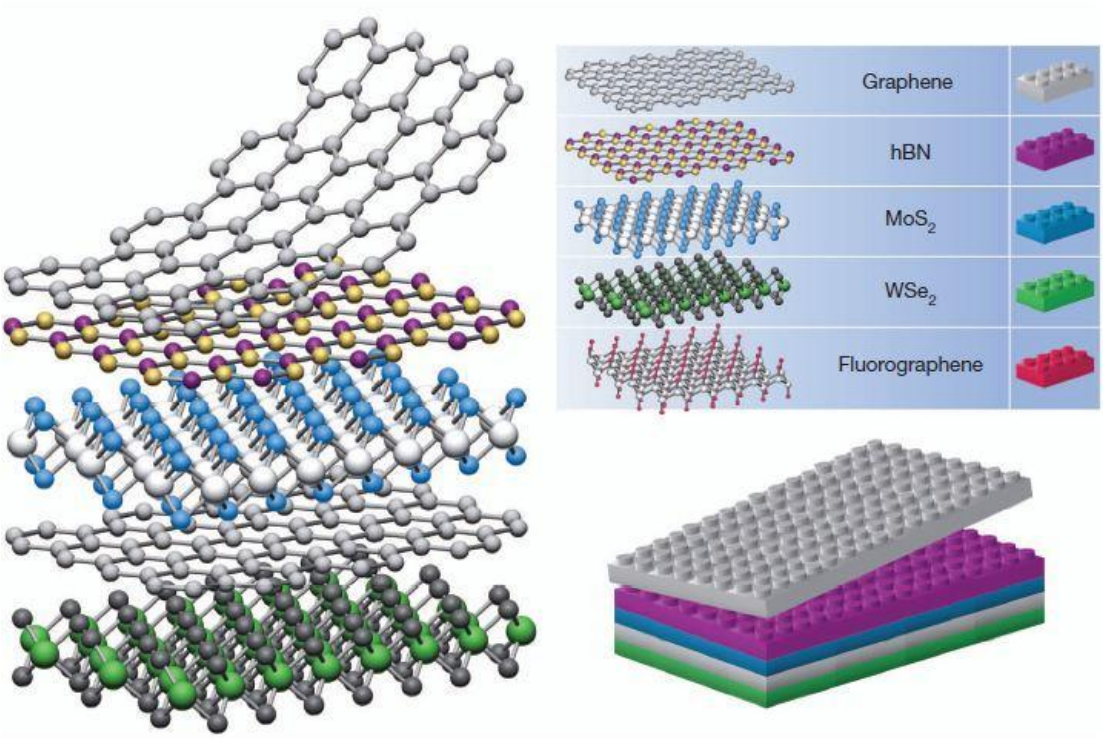

Fig. 1.4 vertical stacking of one material over another that forms heterojunction [5]

Semi-metal/semiconductor heterostructure of Graphene/h-BN/MoS2/ graphene represented by Roy et al [15] has application as FETs which is having electron mobility of 33 cm^2/V-sec and ON/OFF current ratio is more than 10^6 and another semiconductor/semiconductor, WSe2/WS2 heterostructure by nA Duan et al [15][20] has application in solar cell with open-loop voltage of 0.47 v and close loop current on 1.2 nA [18] [20].

MoS_2 based heterostructures have been used in recent years in the production of novel devices for nano-electronic applications. To create a vdW heterostructure, the MoS_2 can be vertically layered, which preserves the electronic and optical properties of each entity while adding new configuration at the interface hence these atomically thin two dimensional atomic structures gives unique electrical, optical and thermal properties which could not be found in there bulk structures For instance, on p-type WSe_2, the n-type MoS_2 monolayer can be layered to create a p-n junction with type-II band alignment. Fang et al. [22] have recently addressed wearable energy sources based on 2-D components, such as paper batteries, supercapacitors and various forms of energy harvesters. Moreover, owing to the metallic property and improved Li and Li_2S adsorption, MoS_2-on-MXene heterostructures can be made in Li-ion batteries.

CHAPTER 2
LITERATURE REVIEW

2.1 Overview

In recent years, since the discovery of the most exciting material, graphene, a great deal of work has been undertaken in the field of nanophotonics. Graphene is the name assigned to a flat carbon mono-layer, closely packed into a two-dimensional (2D) wave grid, leading to a 0 eV bandgap known as graphene without gap. Zero band gap of graphene makes its applications limited like graphene cannot be used digital circuits hence novel approaches were used to find alternatives.

2.2 Summarization of various authors work

In the last few years a prominent work had been done by researchers to replace traditionally used semiconductors like Ge and Si because of their limitations, these materials are no longer capable to cope with today's electronics engineering needs [1] [2] [3] that's why researchers had moved towards Graphene-like two-dimensional materials like TMDCs. TMDs are the semiconductor of type MX_2. Where M are the transition metals and X are the chalcogens. Due to the various permutations of the transit metal and the chalcogens it is possible to generate several various TMDs. TMDs are metallic, semiconductors, semi-metallic, topologic insulators or superconductors. In TMD structures M is transition metal can Molybdenum (Mo-42**)** and tungsten (W-74) and can be any of these elements sulfur(S-16), Tellurium (Te-52), and Selenium (Se-34) among all molybdenite, MoS_2 is the most studied TMDCs monolayer. MoS_2 results in the direct bandgap of 1.80 eV [4] [24] thus this inspiring property of this material is an alternative of gapless graphene and 2D material that can be used in next-generation digital systems and optoelectronics devices. MoS_2 could produce oscillating piezoelectric voltage and current outputs with an odd number of layers, proposing its potential applications in controlling nanodevices and flexible gadgets.

Due to the direct bandgap of 1.80 eV makes MoS_2 a suitable material for switching and optoelectronics nanodevices. A single-layer MoS_2 transistor in Fig.2.1 adopting a hafnium oxide as the gate dielectric material was proposed by B. Radisavljevic's group in 2011 that reported mobility of single-layer MoS_2 up to 200 cm^2 /(V- s) at room temperature with the

current on/off ratio to be 1×10^8 [24]. Later in 2012, for the first time, Zongyou Yin's group recorded the switching character of this system, with photocurrent generation and annihilation within only 50 m-s.

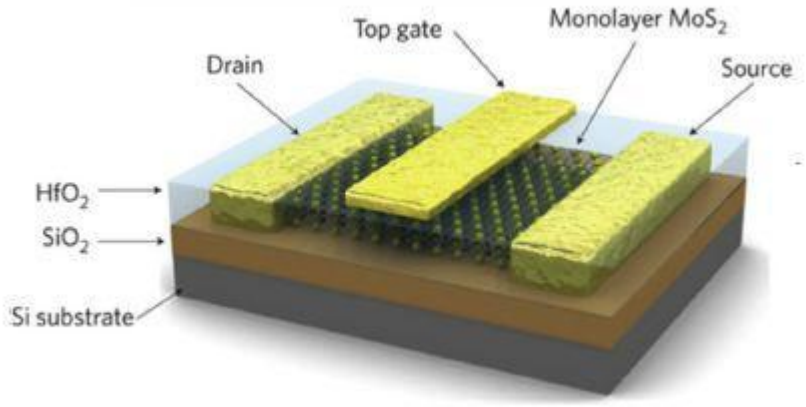

Fig. 2.1 Single-layer MoS_2 as channel-based MOSFET [24]

In the last 10 years the use of large bandgap semiconductors including X rays and radiation detectors in various medical applications has been arousing interest in CdZnTe [19]. Traditional Si and Ge based high-performance spectrometers; CdTe and CdZnTe detectors demonstrate high detection efficiency and good performance at room temperature and are best optional for the development of lightweight and accurate detection systems. A comprehensive survey on the material properties of CdTe and CdZnTe have been proposed by Stefano Del [17] [19]

The most encouraging materials for radiation finders with great energy goal, high discovery execution and action at room temperature are CdTe and CdZnTe. Silicon (Si) and germanium (Ge) are conventional semiconductors used for radiation detectors providing good performance in a various variety of applications [19], the growing area of application has stimulated the development of compound semiconductor-based detectors. A major benefit of compound semiconductors is the ability to develop materials with a wide variety of physical properties (bandgap and atomic number) making them ideal for almost any application.

Rather than Si and Ge, interest in radiation finders working at room temperature has offered ascend to the making of accumulate semiconductors with huge band gaps. In addition, compound semiconductors with large atomic numbers were favored for X-ray and gamma-ray detection to highlight photoelectric interaction. Compound semiconductors

are normally derived from elements in the periodic table of groups III and V (e.g. GaAs) and groups II and VI (e.g. CdTe). Ternary materials have also been developed in addition to binary compounds, e.g. CdZnTe as well as CdMnTe. Table 1.1 displays the physical properties of the most typical semiconductors used to measure radiation.

While CdZnTe or CZT is better known as an X-and gamma-ray detector material for room temperature compound semiconductors. However, the widespread deployment of this substance in large volume CZT detectors is still constrained by the high production cost due to its intrinsic weak thermo-physical properties and above unity segregation coefficient for Zn [14][17] hence CZT has three primary faults compositional inhomogeneity, a high concentrations of dislocation wall /sub grain boundary network and high Te-inclusion / precipitation ratios, which have resulted in a record of selenium being applied to the CZT matrix [14] hence improved compositional homogeneity growth of the new quaternary crystal $Cd_{1-X}Zn_X\ Te_{1-Y}Se_Y$ (CZTS) by the Traveling Heater System (THM) is recorded as a result of reducing the forming of sub-grain boundaries and reducing segregation [14].
The stacking by Van der Waals powers of 2D materials helps the creation of a heterostructure [5][7][8] which is an impressive way of tuning the both optical and electrical properties of individual material an impressive work has been done by Sudhanshu Choudhary [7]. He reported Both MoS_2 and phosphorene reported high absorption rates in the visible region ($\lambda \sim$ 390-430 nm) and in the whole infrared (IR) region, respectively, but after developing the MoS_2 / Phosphorene heterostructure that resulted in the redshift phenomenon with increased absorption coefficient in the whole visible region ($\lambda \sim$ 410 to 780 nm) of the spectrum that finds several potential applications in fabrication of many optoelectronic devices. In 2019 heterostructure of MoS_2/$Hg0.33Cd_{0.66}Te$ was reported by Sudhanshu Choudhary[20] in which the absorption coefficient was observed with increased in the wavelength and also shifts towards the red region of the visible spectrum moreover higher rate of absorption was seen in visible region of the spectrum ($\lambda \sim$640–710 nm) which finds application in optoelectronics devices.

2.3 Conclusion of literature survey

After going through the literature survey it is being concluded, a lot of research is going on 2-D material and their interaction with other material with van der Waal forces of attraction that constitutes heterostructures. Hence vertically stacked heterostructures open various opportunities for various kinds of devices such as photodetectors; spin filtering devices, field-effect transistors [15]. VdW heterostructures have attracted a wide importance from the field of semiconductor devices, material science and physics of matter. Work proposed Sudhanshu Choudhary in papers [7] [20] on vdW heterostructures with MoS2 and others materials opens the door of new optoelectronics which can completely replace the traditional semiconductors

2.4 Research gaps

From the past years two-dimensional layered material has been the prime focus of the researchers after the discovery of graphene years ago in contrast transition dichalcogenides (TMDs), insulating hexagonal di bromide (hBn) consisting of a wide variety of layered material with tunable bandgap and tunable electronic and optical properties despite of making devices from the single material it has been seen in recent years that the researchers are of having more interest in the field of Vander wall heterostructures (vdWHs) enables the new engineering for device design like flexible displays, TMDS based van der walls vertical transistors, vertical tunneling transistors, light-harvesting and detection devices and light-emitting devices.

2.5 Objective of the present work

A heterostructure of cadmium telluride zinc selenium ($Cd_{0.90}Zn_{0.10}Te_{0.93}Se_{0.07}$) and monolayer molybdenum disulfide (MoS_2) is suggested for tuning the optical properties in the visible region both the optical and electronic properties of individual material and heterostructure have been investigated and compared with the individual material, dielectric constant *(η)*, refractive index *(ε)* and optical conductivity have been calculated that gives the confirmation of changes in the value of absorption coefficient in changing the values of dielectric constant *(η)* and refractive index *(ε)* and also it was found that absorption shifted to visible region completely in $MoS_2/Cd_{0.90}Zn_{0.10}Te_{0.93}Se_{0.07}$ heterostructure as compared to its constituent.

CHAPTER 3

Setup and simulations

3.1 Computational details for MoS_2

By Atomistix Tool Kit (ATK) with first-principle approach based density functional theory (DFT) used for the measurement of the electronic and optical properties of MoS_2. The DFT measurements taken here reflect the exchange-correlation energy approximation (MGGA) of Perdew-Burke-Ernzerhofer (PBE) [24] [25]. The 9x9x1 Brillouin-zone study Monkhorst-pack scheme along with the 150-rydberg energy cut is used [26].

3.1.1 Geometry structure and stability of MoS_2

Fig.3.1 shows the geometry structure monolayer MoS_2. The lattice parameters calculated are a=3.16 with α, β are 90 degrees and γ is 120 degree and bond length in Mo-S is 2.42 Å and bond angle of 81.63 degrees. Each MoS_2 type has a layered structure in which planes of sulfide ions sandwich a plane of molybdenum. The stacked monolayer, maintained by weak vdW interactions, consists of Bulk MoS_2.

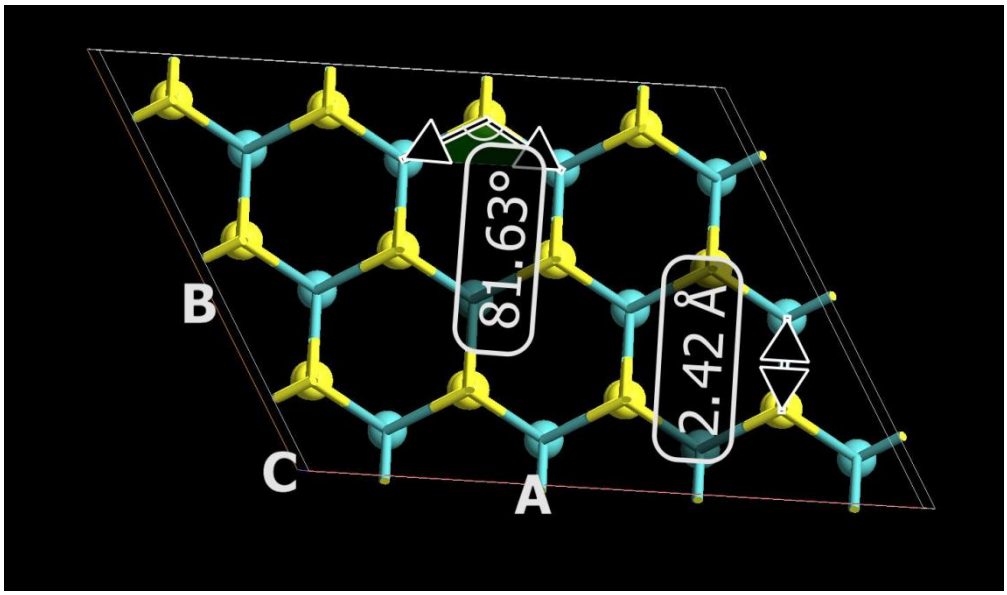

Fig. 3.1 Monolayer bulk structure of MoS_2

3.2 Computational details for $Cd_{0.90}Zn_{0.10}Te_{0.93}Se_{0.07}$

For $Cd_{0.90}Zn_{0.10}Te_{0.93}Se_{0.07}$ compound DFT based simulations are performed on Atomistix Tool Kit (ATK). Atomic positions are relaxed with force tolerance of 0.05 eV/ Å using LBFGS algorithm. Moreover optimized geometry is sampled by 12 ×12×1 in x-y-z coordinates Monk horst-Pack Scheme is used along with mesh cut-off energy of 150 Rydberg.

3.2.1 Geometry structure and stability of $Cd_{0.90}Zn_{0.10}Te_{0.93}Se_{0.07}$

Relaxed geometry of $Cd_{0.90}Zn_{0.10}Te_{0.93}Se_{0.07}$ is shown in Fig.3.2 geometry was optimized using LBFGS geometry optimizer until the forces on each atom were lower than 0.05 eV/ Å. Calculated lattice parameters of $Cd_{0.90}Zn_{0.10}Te_{0.93}Se_{0.07}$ are a= 22 Å b=9.23 Å and c= 4.58 Å with α, β, γ =60 degrees.

After relaxing all the atomic positions bond length shifted to minimum strain level that resulted bond length of 2.73Å between Zn-Te, 2.71 Å between Se-Cd and 2.82 Å between Cd-Te has been found in Fig. 3.3.

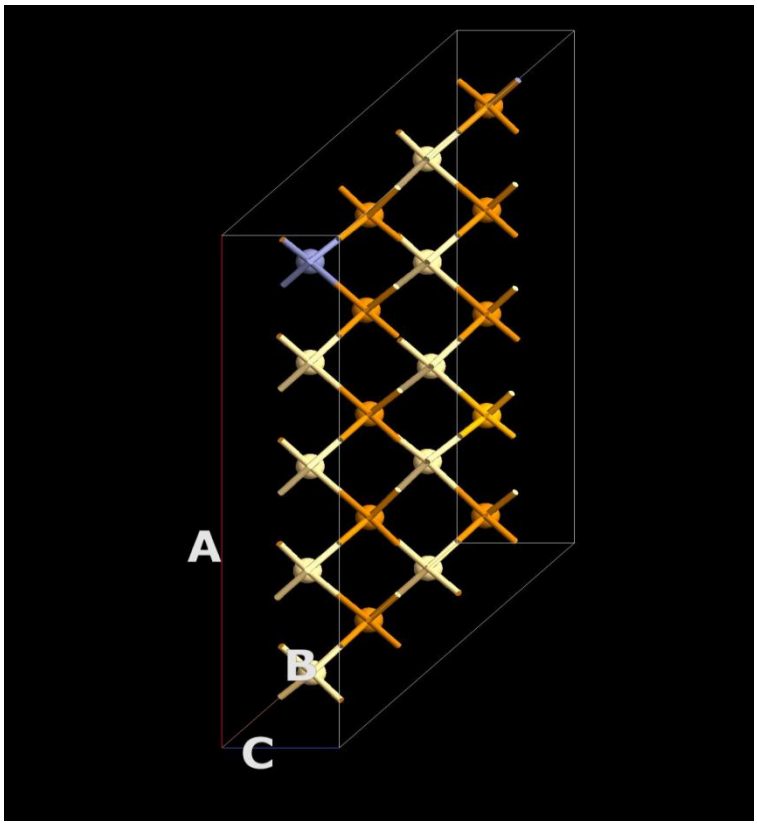

Fig. 3.2 Relaxed geometry of $Cd_{0.90}Zn_{0.10}Te_{0.93}Se_{0.07}$

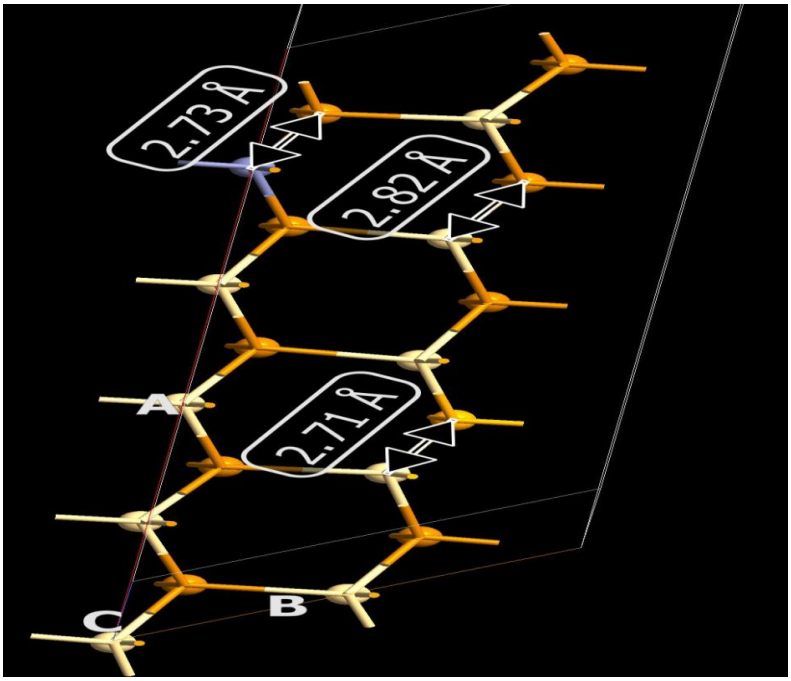

Fig. 3.3 Relaxed geometry of $Cd_{0.90}Zn_{0.10}Te_{0.93}Se_{0.07}$ with bond length

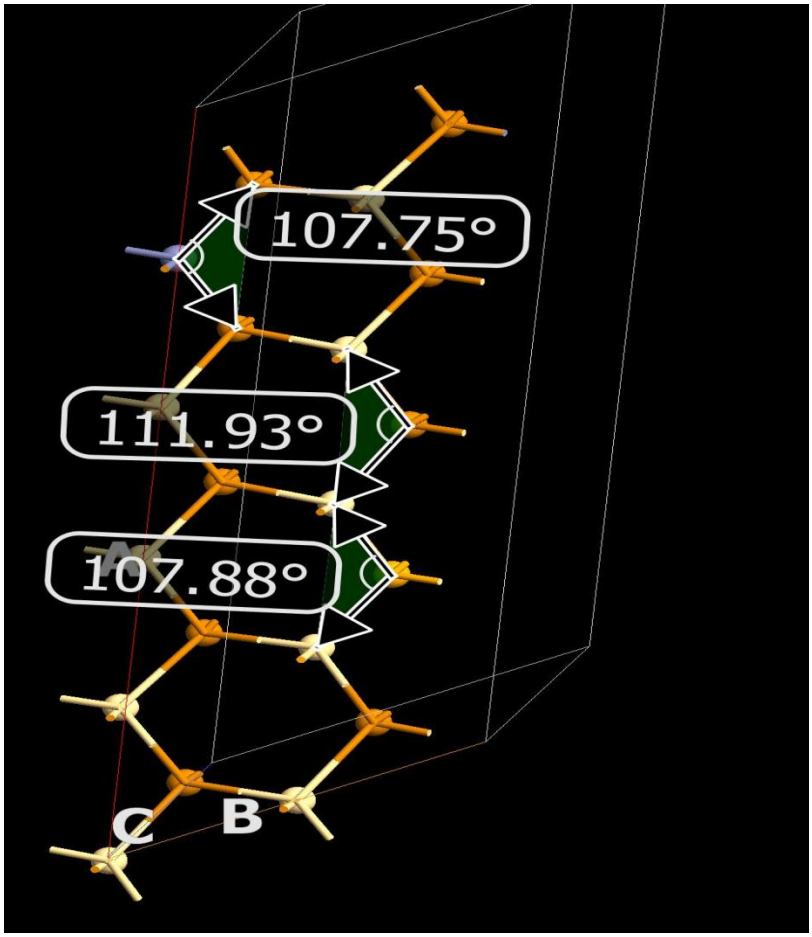

Fig. 3.4 Relaxed geometry of $Cd_{0.90}Zn_{0.10}Te_{0.93}Se_{0.07}$ with bond angles

After relaxing all the atomic positions, bond length shifted to the minimum strain level that resulted in a bond angle of 107.75 degrees between Te-Zn-Te, 111.93 degrees between Cd-Se-Cd, and 107.88 degrees between Cd-Te-Cd is found in Fig. 4.4.

3.3 Computational details for $MoS_2/Cd_{0.90}Zn_{0.10}Te_{0.93}Se_{0.07}$ heterostructure

Simulations based on $MoS_2/Cd_{0.90}Zn_{0.10}Te_{0.93}Se_{0.07}$ heterostructure, DFT are performed on the ATK. A force tolerance of 0.05 eV / Å with LBFGS-Algorithm is added to the atomic positions. Furthermore, the optimized geometry of the x-y-z coordinate samples is sampled at 15 × 15 × 1 in the Monk horst-Pack System, with a 150 Rydberg mesh cut-off. Similar to the VdW interactions not defined in the Regular PBE function, semi-empirical Grimme DFT-D2 correct was chosen to define. The combination of DFT and MGGA will assess the optical properties and sample the Brillouin area from 15 × 15 × 1k sampling points 28]**.**

3.3.1 Geometry structure and stability of $MoS_2/Cd_{0.90}Zn_{0.10}Te_{0.93}Se_{0.07}$ heterostructure

Vertically stacked layer of monolayer MoS_2 that is interacted with $Cd_{0.90}Zn_{0.10}Te_{0.93}Se_{0.07}$ by vdW force of attraction all atomic positions are relaxed with force tolerance 0.05 eV/°A using LBFGS algorithm having a strain of 2.5%. Which results in the bonds lengths and angles discussed below in Fig. 3.6 and Fig. 3.7.

After relaxing all the atomic positions, bond length shifted to a minimum strain level of 2.5% that resulted in a bond length of 2.60Å between Zn-Te, 2.58 Å between Se-Cd and 2.78 Å between Cd-Te.

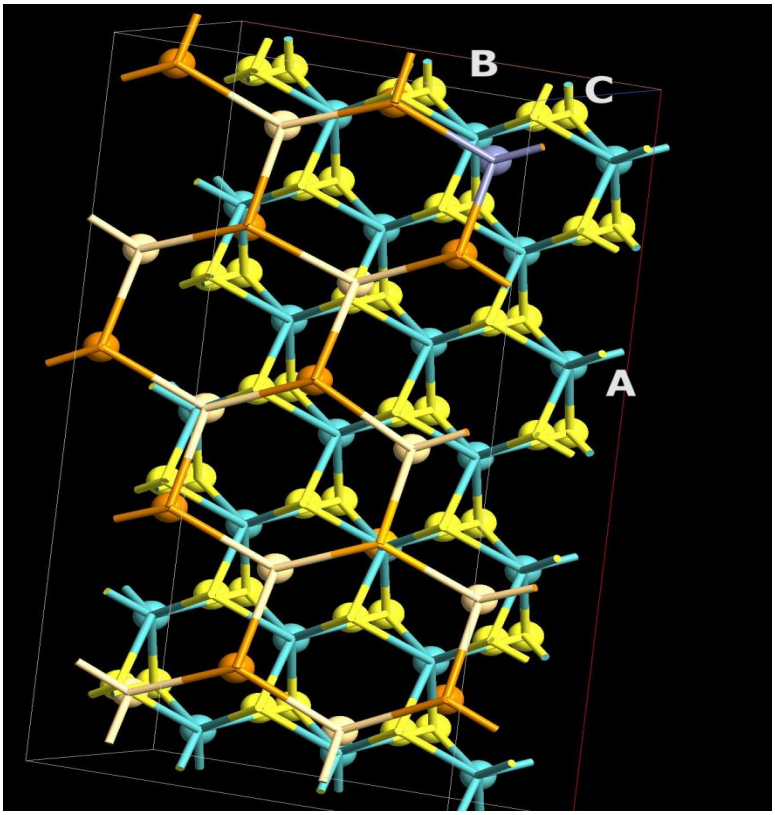

Fig.3.5. Relaxed geometry of $MoS_2/Cd_{0.90}Zn_{0.10}Te_{0.93}Se_{0.07}$ heterostructure in XY plane

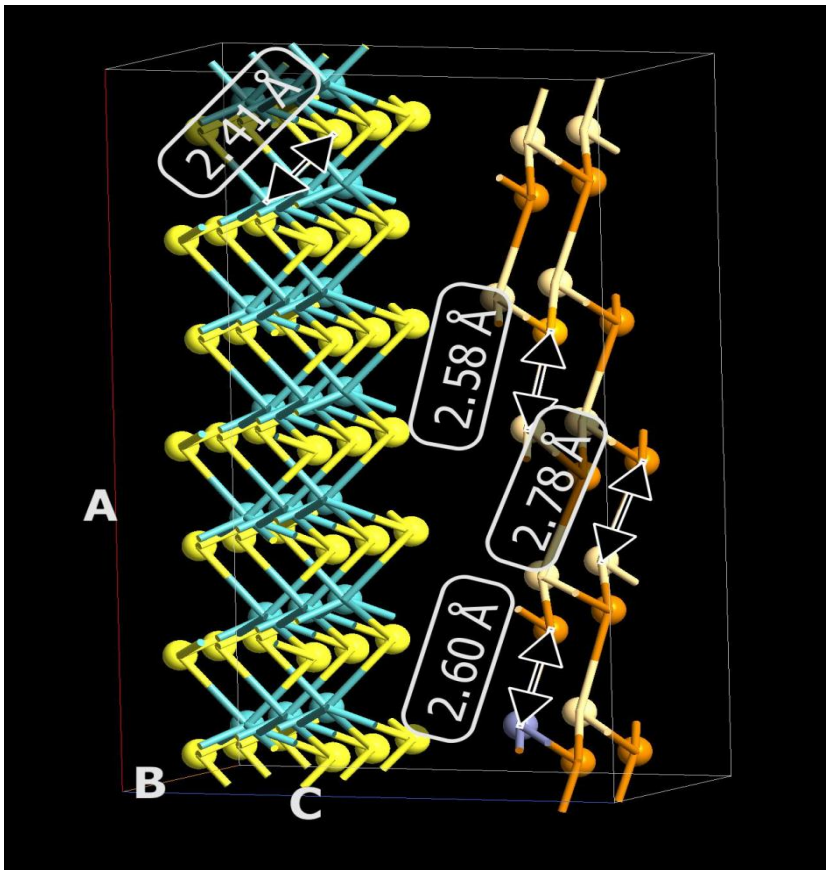

Fig. 3.6 Relaxed geometry of $MoS_2/Cd_{0.90}Zn_{0.10}Te_{0.93}Se_{0.07}$ heterostructure with bond length

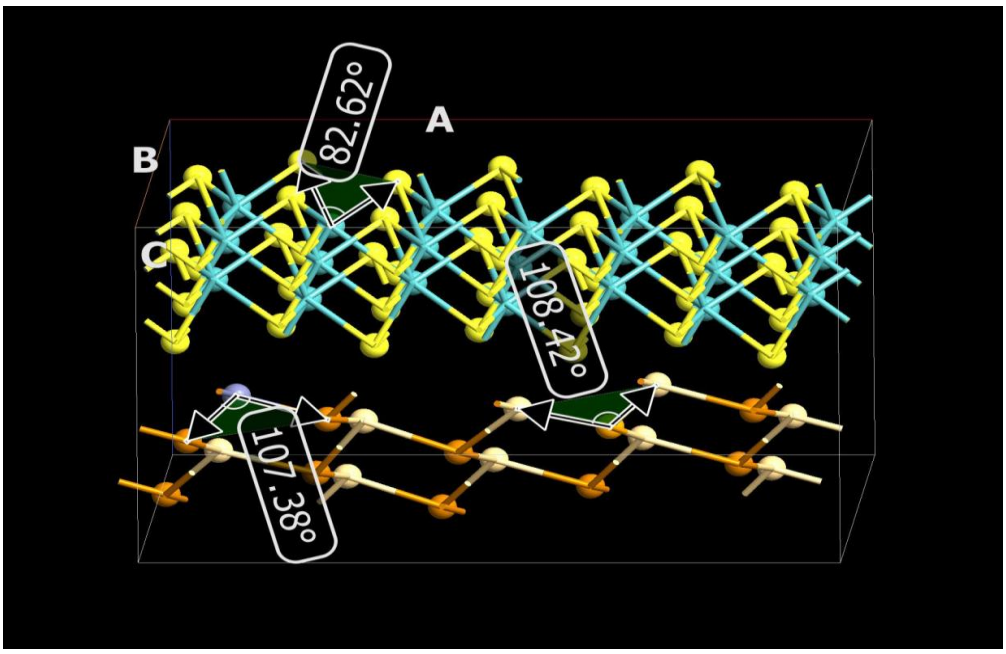

Fig. 3.7 Relaxed geometry of MoS_2/ $Cd_{0.90}Zn_{0.10}Te_{0.93}Se_{0.07}$ heterostructure with bond angles in XZ plane

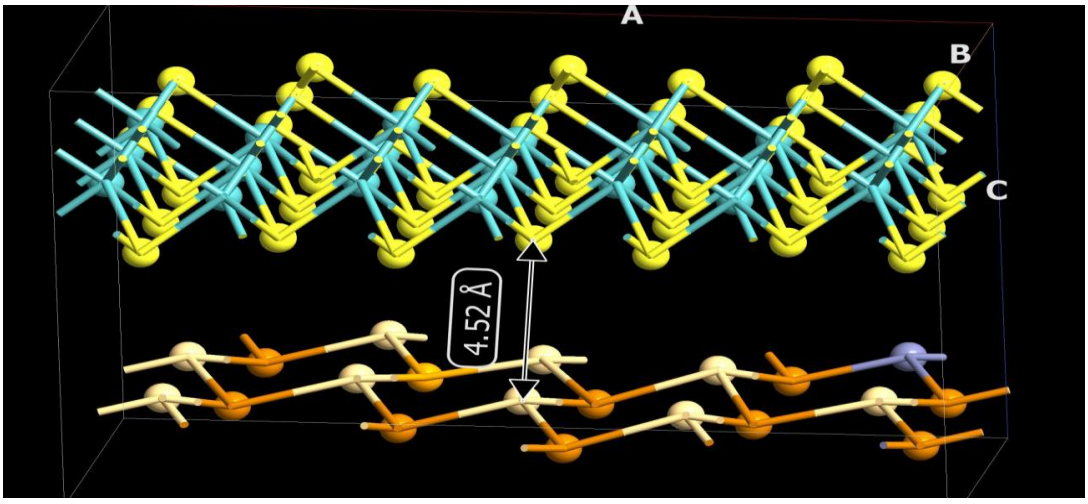

Fig. 3.8 Relaxed heterostructure of MoS2/$Cd_{0.90}Zn_{0.10}Te_{0.93}Se_{0.07}$, Interlayer distance between MoS_2 and $Cd_{0.90}Zn_{0.10}Te_{0.93}Se_{0.07}$.

After relaxing all the atomic positions, bond angles shifted to a minimum strain level of 2.5% that results in a bond angle of 107.38° between Te-Zn-Te, 108.42° between Cd-Se-Cd and 82.62° between Te-Cd-Te is shown in Fig. 3.7.

Relaxed geometry shows the minimum strain level of 2.5% that confirms the minimum lattice mismatching. Hence total binding energy was calculated to get the most favorable heterostructure. $E_B = \frac{E-(E_1+E_2)}{N}$, E_1 and E_2 represent the free standing energy of MoS_2 and $Cd_{0.90}Zn_{0.10}Te_{0.93}Se_{0.07}$ respectively and E gives the free-standing energy of $MoS_2/Cd_{0.90}Zn_{0.10}Te_{0.93}Se_{0.07}$, N gives the total no. of free electrons of the heterostructure. Fig.3.9 gives the interlayer distance v/s binding energy of the heterostructure.

Total energies are calculated at different interlayer distances of the heterostructure then E_B is calculated by the above formula given.

Interlayer distance (Å)	E (eV)	E_1(eV)	E_2(eV)	E_B(eV)/atom
4.11	-117028.0778	-2428.437	-48598.685	-809.650
4.32	-117028.0850	-2428.437	-48598.685	-809.750
4.52	-117028.1152	-2428.437	-48598.685	-809.850
4.72	-117028.0950	-2428.437	-48598.685	-809.720
4.91	-117028.0810	-2428.437	-48598.685	-809.450

Table 3.1 Total binding energy of heterostructure and of its constituent.

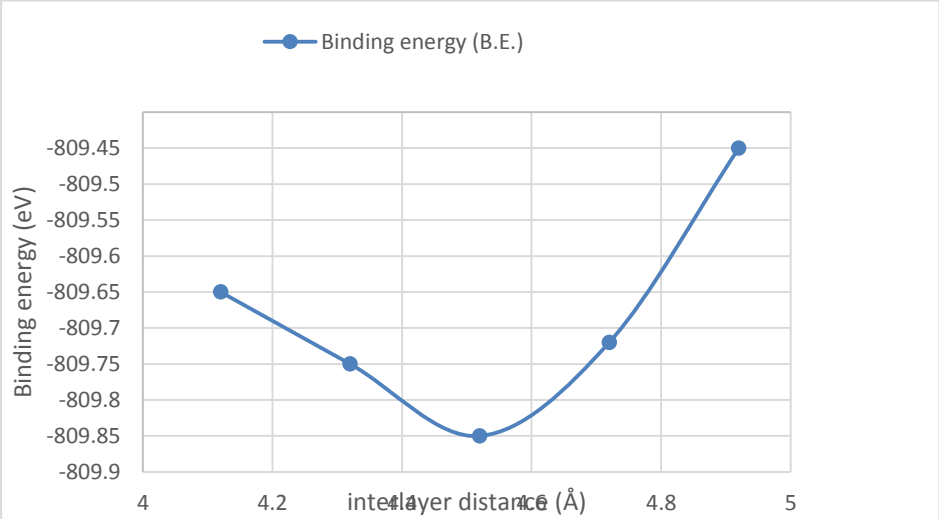

Fig. 3.9 Interlayer distance v/s Binding energy

Total energy has been calculated and represented in table 3.1. That gives the most negative energy of -809.8598 eV per atom of the heterostructure that shows at interlayer distance of 4.52 Å most stable heterostructure with strong vdW interaction between two monolayers.

CHAPTER 4

Results and Analysis

4.1 Electronic properties

4.1.1 Electronic properties of MoS_2

Monolayer MoS_2 is having totally different properties than the bulk while monolayer shows the direct bandgap of energy on the other hand bulk shows an indirect bandgap. A single layer of MoS_2 absorbs 10% of the incident radiation while compared to bulk it can yield on 0.4% while the bandgap this material is highly tunable by adding the additional layers[22].

By Atomistix Tool Kit (ATK) with first-principle approach based DFT used for the measurement of the electronic and optical properties of MoS_2. A MGGA of Perdew-Burke-Ernzerhofer (PBE) to describe the exchange-correlation efficiency is a DFT calculation adopted here. [24] [25] M-P scheme with 9x9x1 Brillouin-zone sampling along with energy cut-off of 150 Rydberg is selected [26].

4.1.2 Band structure of MoS_2

The band structure is very important in understanding the properties of materials and finding possible applications. Band structure of MoS_2 exhibits quite unique properties as its changes from direct band to indirect bandgap as the material changes from monolayer to multilayer has been investigated in [24].

The solid band structure describes the energy continuum that electrons can possess within the solid and the energy continuum states that they do not possess. The electrons in the solid will only hold a certain range of energy in certain positions in the band configuration because of quantum mechanical wave functions.

The repetitiveness of the periodic lattice defined by the Brillouin zone makes it possible to reflect the band structure of the whole solid by using the band structure of a lattice. To describe many critical physical properties, the band theory has been used and is necessary in designing all electrical devices.

A thorough investigation of the electronic structure of all TMDs has been investigated by first-principles calculations [28] and their results are studied for future applications. Fig. 4.1 shows the band structure of monolayer MoS_2 that result in a direct bandgap of 1.81 eV.

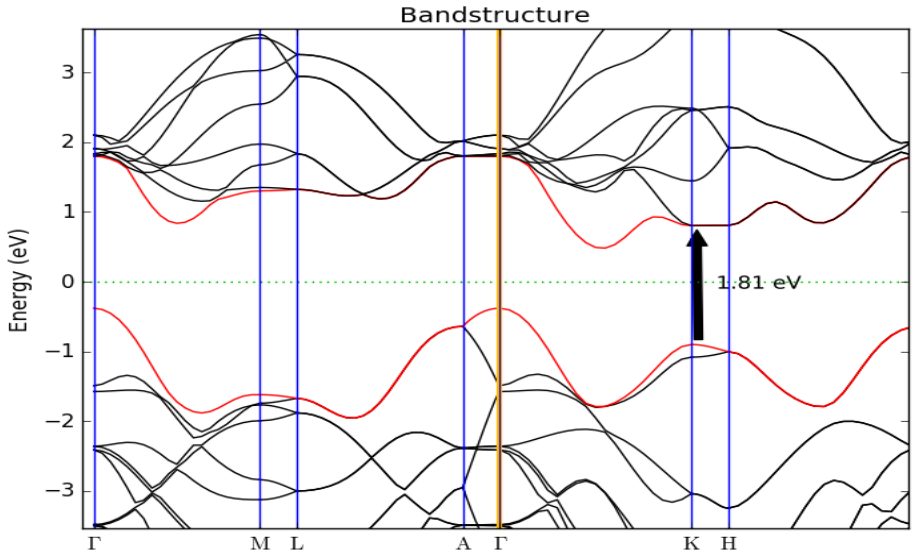

Fig. 4.1 Band structure of monolayer MoS_2, Eg=1.81eV

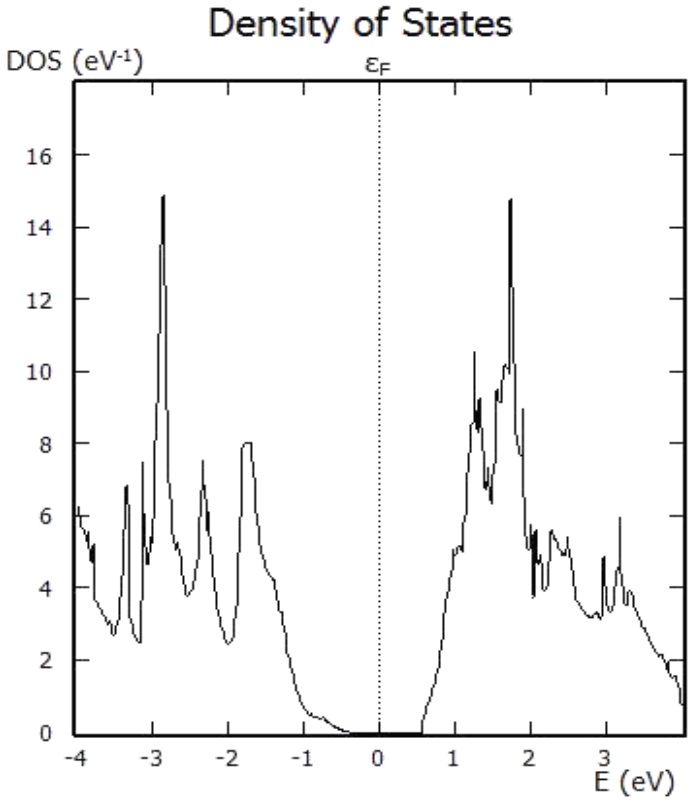

Fig. 4.2 Density of states of MoS_2

4.1.3 Electronic property of $Cd_{0.90}Zn_{0.10}Te_{0.93}Se_{0.07}$

Electronic properties of $Cd_{0.90}Zn_{0.10}Te_{0.93}Se_{0.07}$ compound (DFT) based simulations are performed on Atomistix Tool Kit (ATK). Atomic positions are relaxed with a force tolerance of 0.05 eV/ Å using LBFGS algorithm. Moreover relaxed geometry is sampled by 12 ×12×1 in x,y and z coordinates Monk horst-Pack Scheme is used along with mesh cut-off energy of 150 Rydberg.

The bandgap of $Cd_{1-x}\,Zn_{\,x}\,Te_{1-y}\,Se_{\,y}$ is computed by using the formula given below

$Eg_{x,y} = 1.511 - 0.54y + 0.6x\ (x, y \leq 0.10)$

Where x and y are the molar fraction of Cadmium and E_g is the energy gap conformed to ref. [17].

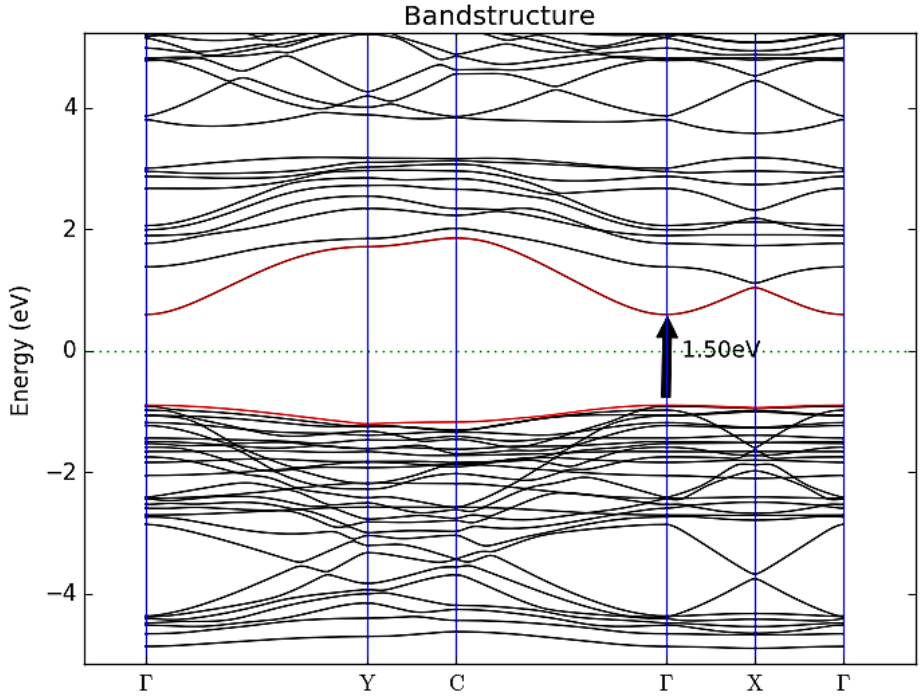

Fig. 4.3 Band structure of $Cd_{0.90}Zn_{0.10}Te_{0.93}Se_{0.07,}$ Eg=1.501 eV

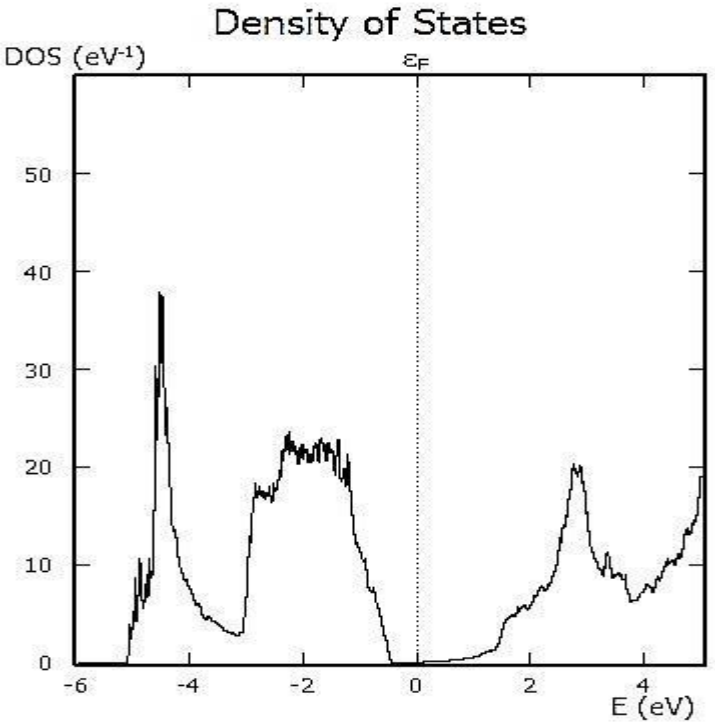

Fig. 4.4 DOS of $Cd_{0.90}Zn_{0.10}Te_{0.93}Se_{0.07}$

4.1.4 Electronic property of $MoS_2/Cd_{0.90}Zn_{0.10}Te_{0.93}Se_{0.07}$

The Atomistix Tool Kit (ATK) performs electronic properties of $MoS2/Cd_{0.90}Zn_{0.10}Te_{0.93}Se_{0.07}$ heterostructure; DFT based simulations. With a force resistance of 0.05 eV / Å using the LBFGS algorithm, the atomic positions are relaxed. In addition, optimized geometry is sampled by 15× 15× 1 in x-y-z coordinates. The Monk horst-Pack Scheme is used along with 150 Rydberg [26][27] mesh cut-off energy. Semi-empirical Grimme DFT-D2 corrections were chosen to describe the VdW interactions that are not specified in the regular PBE function.

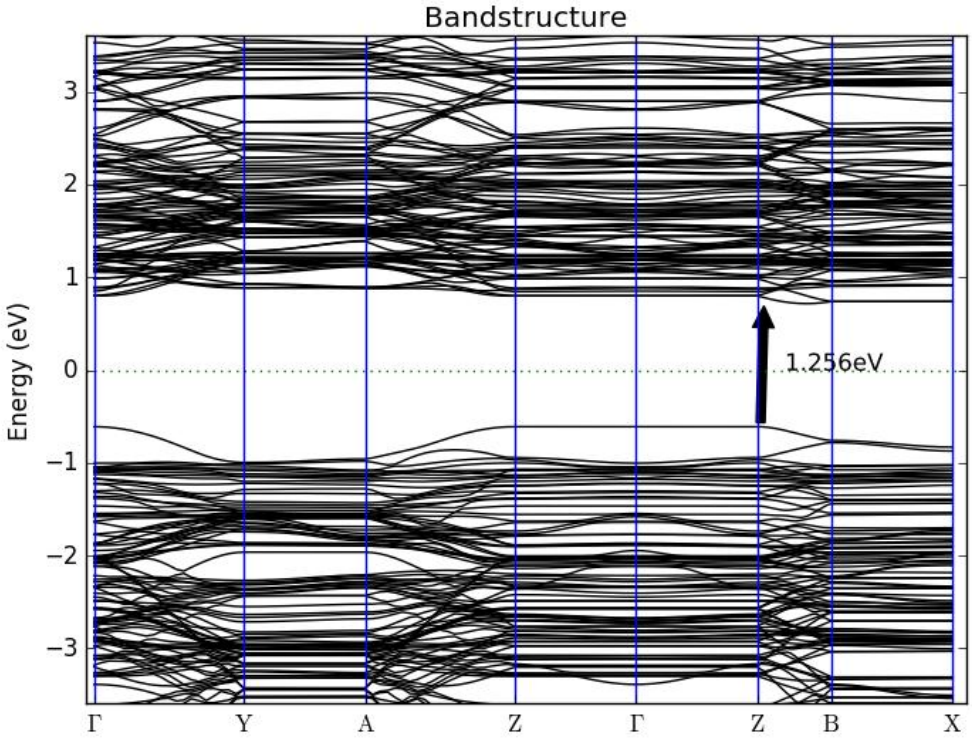

Fig. 4.5 Band structure of $MoS_2/Cd_{0.90}Zn_{0.10}Te_{0.93}Se_{0.07}$

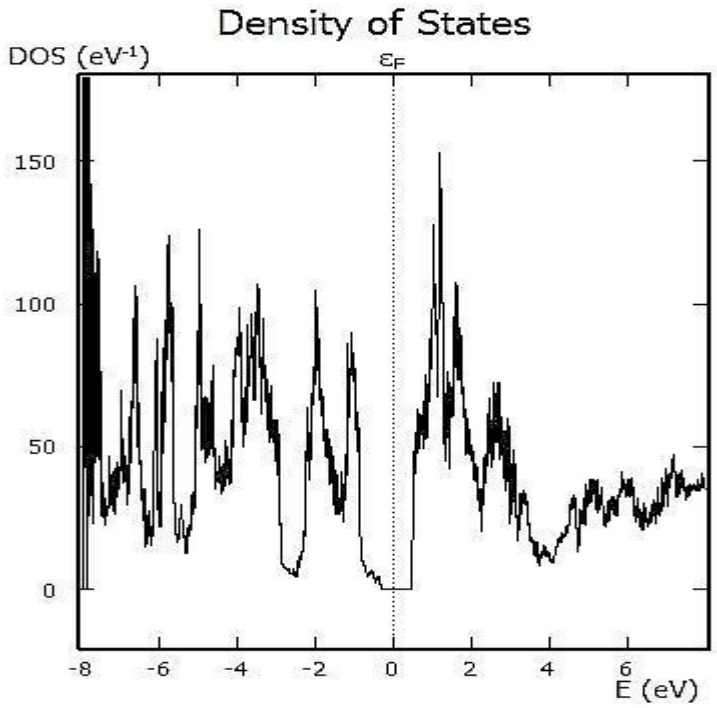

Fig. 4.6 Density of states (DOS) for $MoS_2/Cd_{0.90}Zn_{0.10}Te_{0.93}Se_{0.07}$.

4.2 Optical properties

4.2.1 Optical properties of MoS_2

Optical characteristics are obtained using DFT in conjunction with the Tran and Blaha meta-GGA (TB09) [27].For the measurement of optical properties using 15x15x1 k-points sampling, the Brillouin region is sampled. The expansion is adjusted to 0.05 eV in order to account for the thermal effect on the structure's optical properties**.**

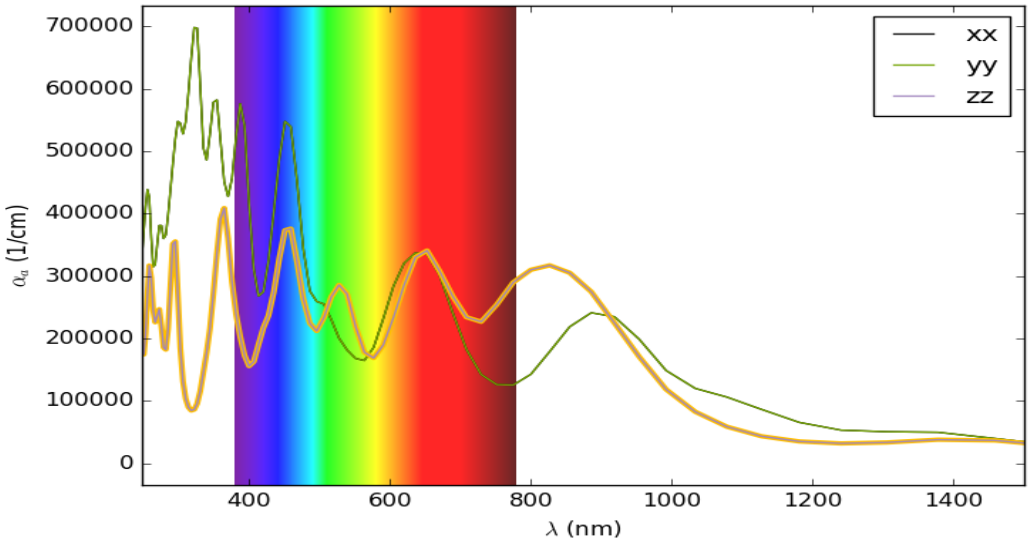

Fig. 4.7 Absorption coefficient v/s wavelength of MoS_2

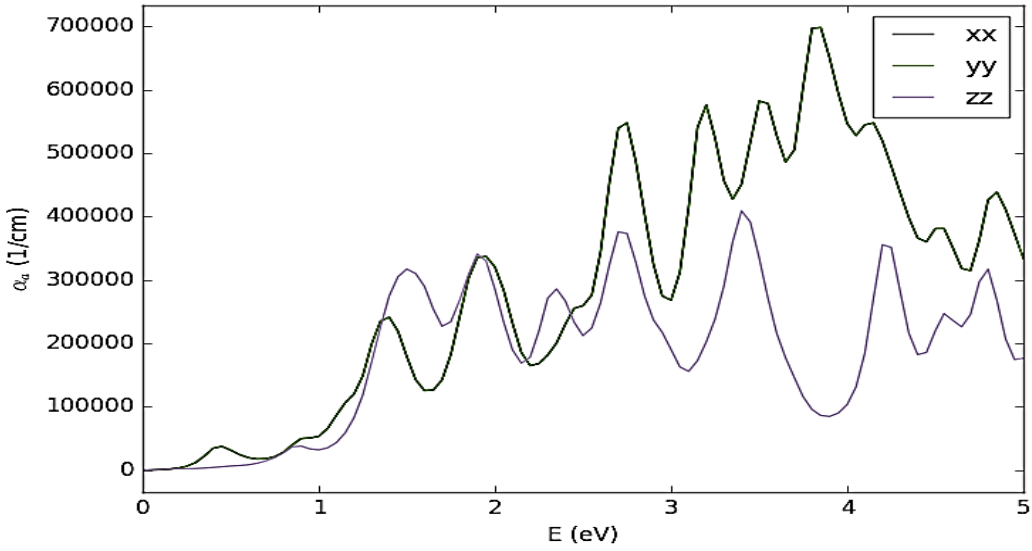

Fig. 4.8 Absorption coefficient v/s Energy of MoS_2

Above Figure 4.8 shows the strongest peak near ~3.8 eV similarly in Fig 4.7 absorption coefficient v/s wavelength of MoS_2 much of the absorption lies near the blue region of the visible region.

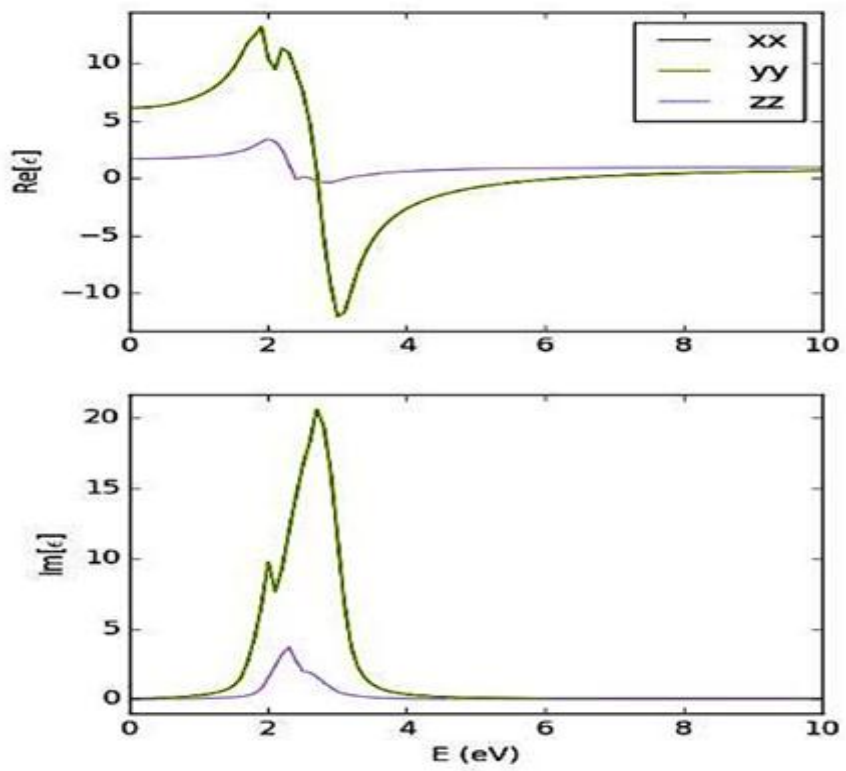

Fig. 4.9 Real (ε_1) and imaginary(ε_2) part of dielectric constant v/s energy of MoS_2

4.2.2 Optical properties of $Cd_{0.90}Zn_{0.10}Te_{0.93}Se_{0.07}$

Optical properties of $Cd_{0.90}Zn_{0.10}Te_{0.93}Se_{0.07}$ DFT based calculations are conducted on the ATK. Atomic positions are relaxed using the LBFGS equation with a force resistance of 0.05 eV / Å. In addition, relaxed geometry is sampled by 12×12×1 in x-y-z coordinates The Monk Horst-Pack Scheme is used along with 150 Rydberg mesh cut-off energy.

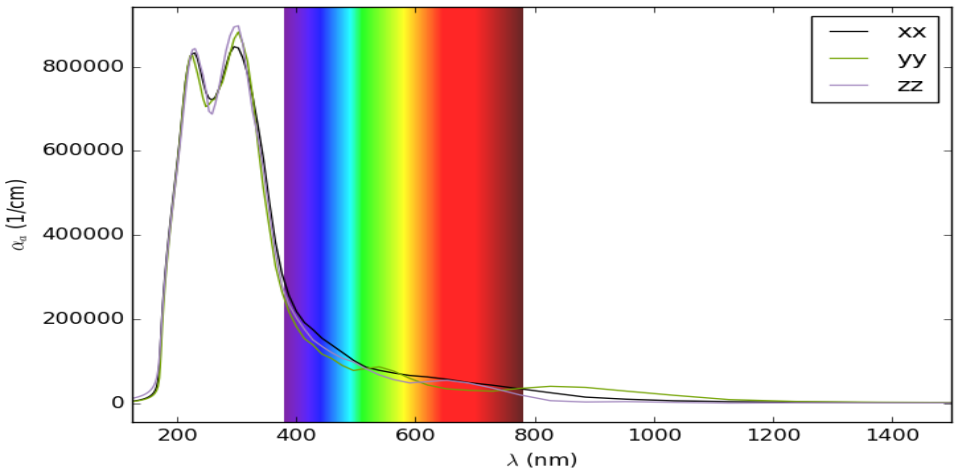

Fig.4.10 Absorption coefficient v/s wavelength of $Cd_{0.90}Zn_{0.10}Te_{0.93}Se_{0.07}$

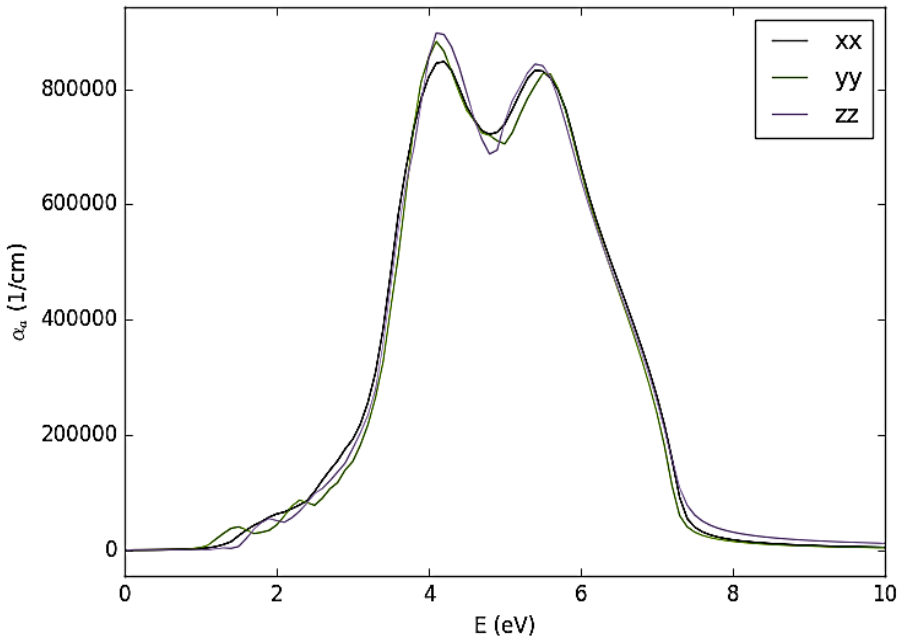

Fig. 4.11 Absorption coefficient v/s Energy of $Cd_{0.90}Zn_{0.10}Te_{0.93}Se_{0.07}$

Above Fig. 4.11 that shows the absorption coefficient v/s Energy of $Cd_{0.90}Zn_{0.10}Te_{0.93}Se_{0.07}$ and wavelength in Fig. 4.10 one of the peak is at 4 eV and the other peak is at 5.8 eV and strong absorption can be seen from (*λ~ 130nm-250nm)*

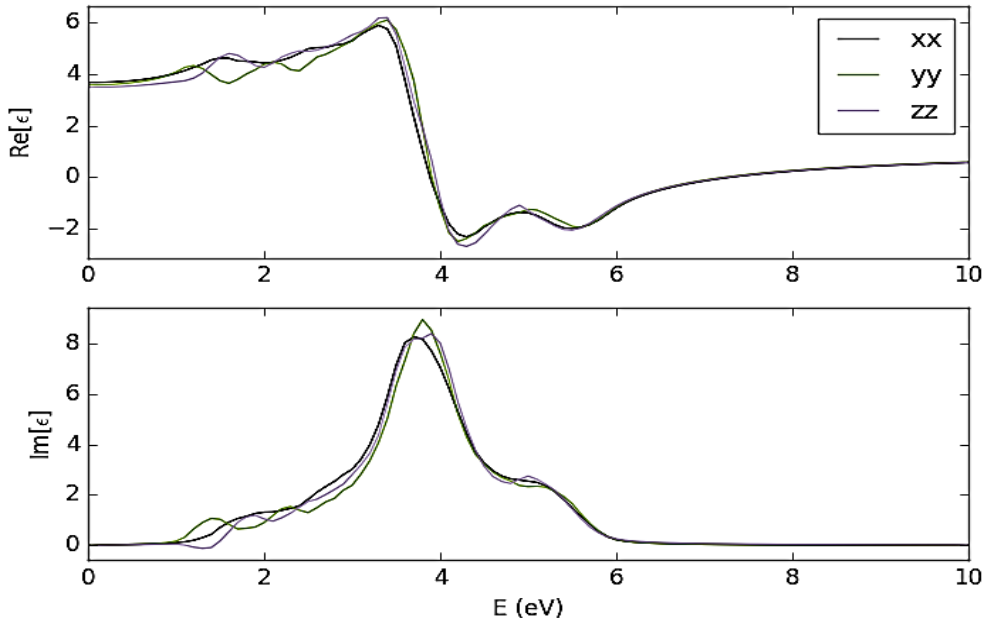

Fig. 4.12 Real (ε_1) and imaginary (ε_2) part of dielectric (ε) function v/s Energy

$Cd_{0.90}Zn_{0.10}Te_{0.93}Se_{0.07}$

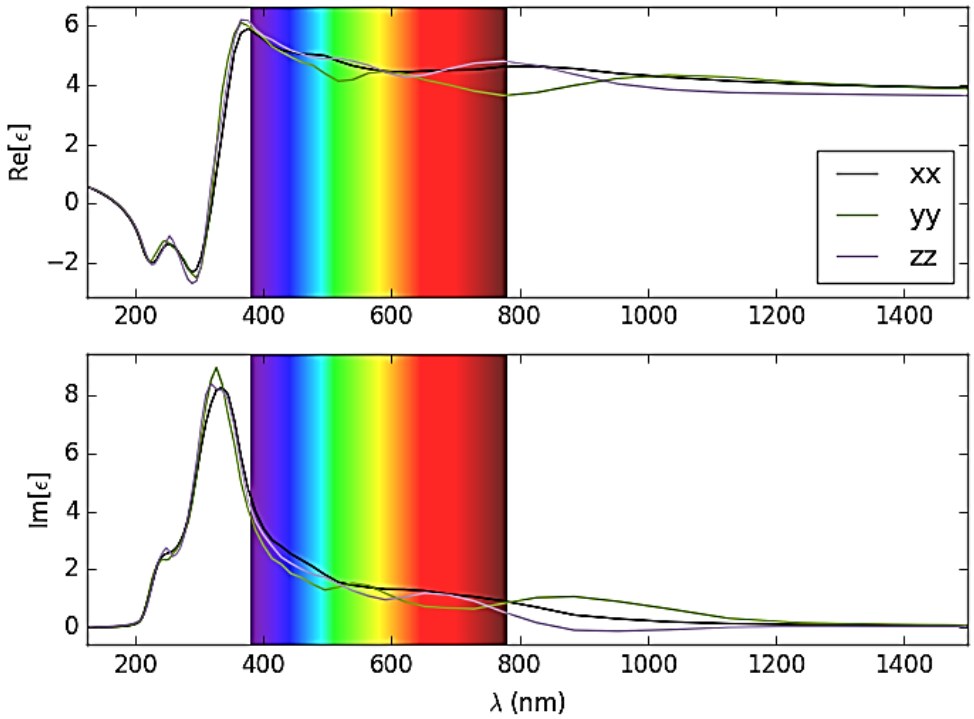

Fig. 4.13 Real (ε_1) and imaginary (ε_2) part of dielectric function (ε) dielectric function v/s Wavelength $Cd_{0.90}Zn_{0.10}Te_{0.93}Se_{0.07}$

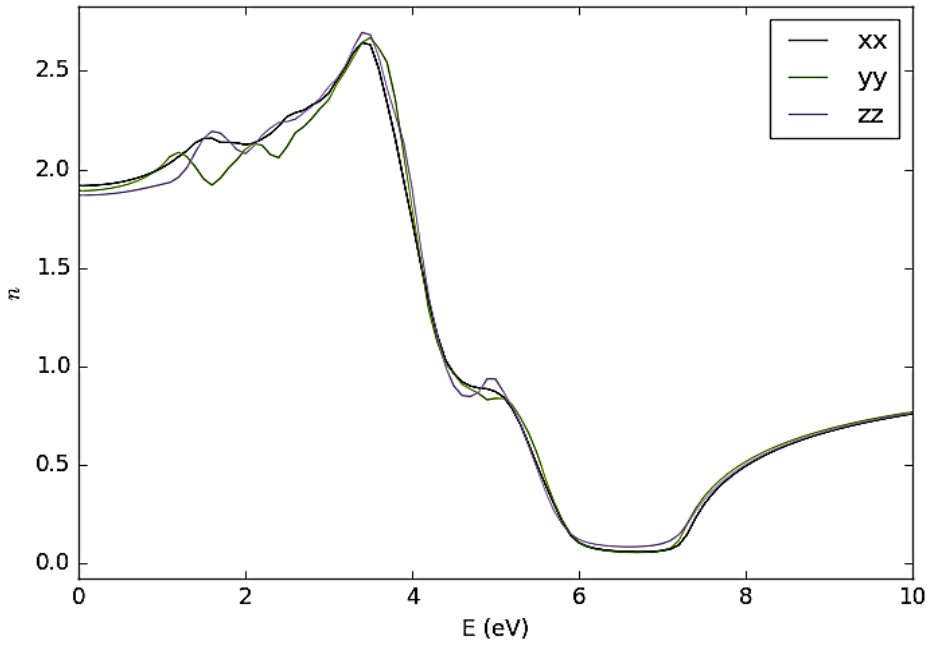

Fig. 4.14 Refractive index v/s Wavelength $Cd_{0.90}Zn_{0.10}Te_{0.93}Se_{0.07}$

4.2.3 Optical properties of $MoS_2/Cd_{0.90}Zn_{0.10}Te_{0.93}Se_{0.07}$ heterostructure

ATK software was used to find the optical properties of $MoS_2/Cd_{0.90}Zn_{0.10}Te_{0.93}Se_{0.07}$ heterostructure DFT based simulations. With a force resistance of 0.05 eV/ Å using the algorithm LBFGS, the atomic positions are relaxed. In addition, 15×15×1 k points in x-y-z coordinates are sampled for optimized geometry. Along with the 150 Rydberg mesh cut-off energy, the Monk horst-Pack Scheme is used. Semi-empirical Grimme DFT-D2 corrections were selected to describe the VdW interactions that are not described in the standard PBE function. Optical properties are determined and the Brillouin region is sampled by integrating DFT with MGGA using 15 × 15× 1 k points sampling [28].

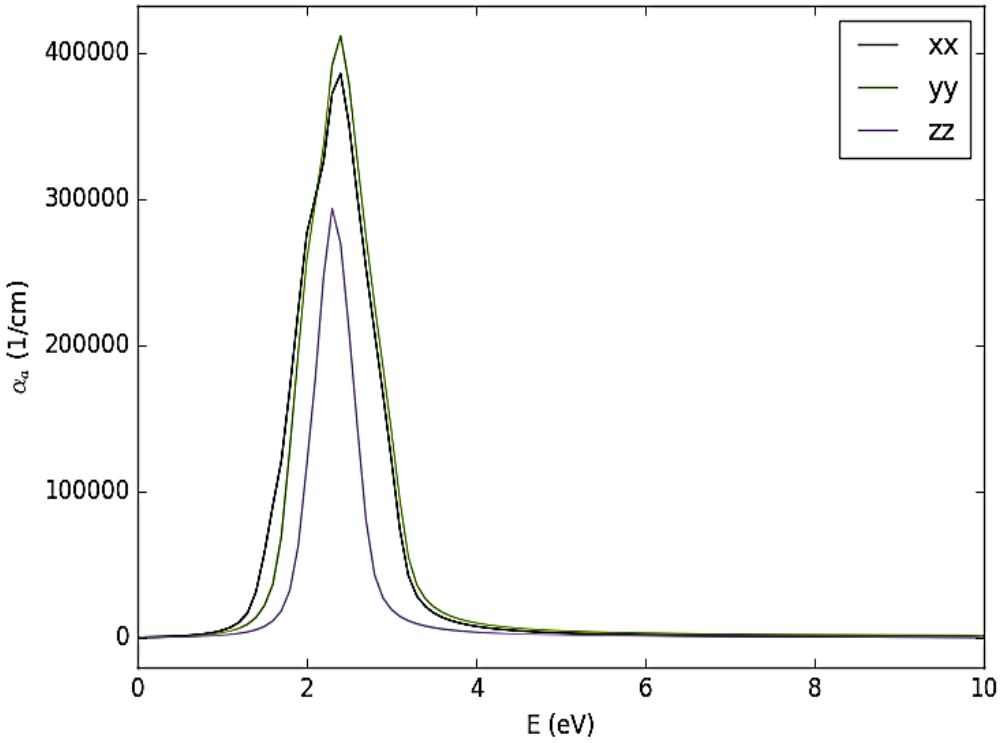

Fig. 4.15 Absorption coefficient v/s energy of MoS_2/ $Cd_{0.90}Zn_{0.10}Te_{0.93}Se_{0.07}$

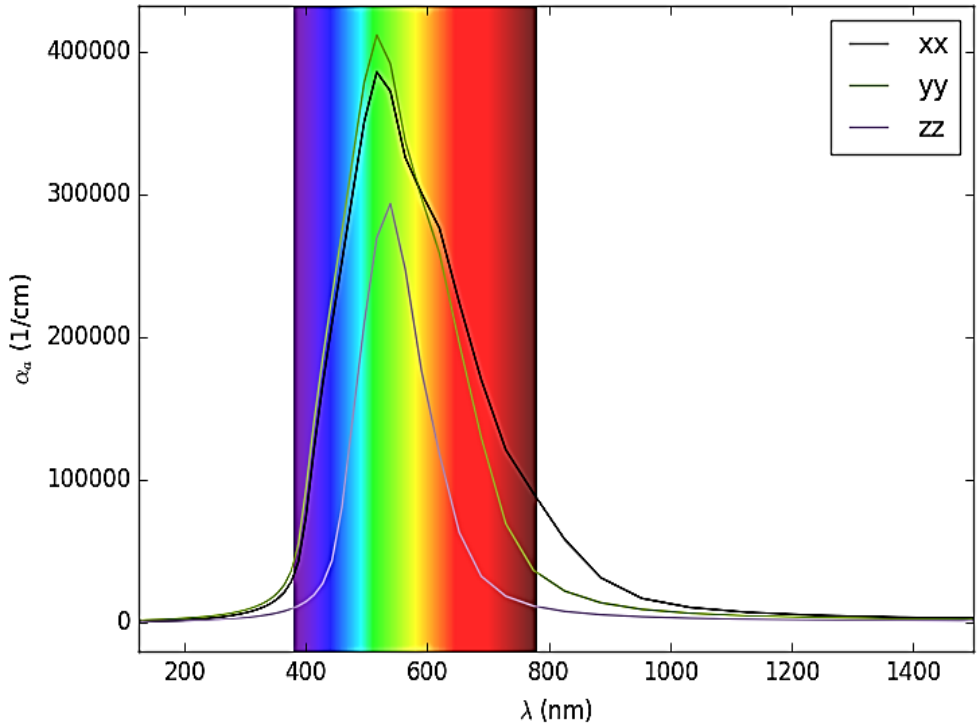

Fig. 4.16 Absorption coefficient v/s wavelength of MoS_2/ $Cd_{0.90}Zn_{0.10}Te_{0.93}Se_{0.07}$

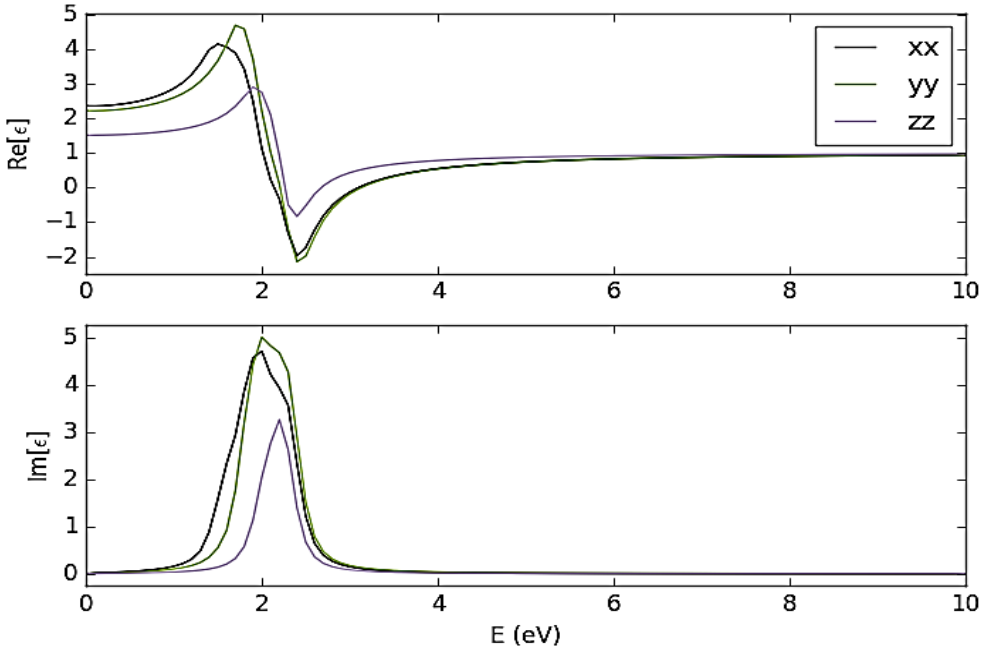

Fig. 4.17 Real (ε_1) and imaginary (ε_2) part of dielectric function v/s energy of $MoS_2/Cd_{0.90}Zn_{0.10}Te_{0.93}Se_{0.07}$

For the measurement of susceptibility the relative dielectric constant (ε_r), the polarizability 'α' and optical conductivity (σ) are used [20]

To measure the susceptibility, the equation below, was used with the Kubo-Greenwood method

$$\chi_{i,j}(\omega) = -\frac{e^2\hbar^4}{\varepsilon_0 m^2\omega^2 V}\sum_{nm}\frac{f(E_m)-f(E_n)}{E_{mn}-\hbar\omega-i\Gamma}\,\pi^i_{nm}\pi^j_{nm} \quad (1)$$

Where f the Fermi function, π^i_{nm} is the i_{th} component of the dipole matrix element between state n and m and Γ the broadening and V is the volume.

$$\varepsilon_r = 1+\chi(\omega) \quad (2)$$

$$\sigma(\omega) = -Img\,(\omega\,\varepsilon_0\chi(\omega)) \quad (3)$$

$$\alpha(\omega) = V\,\varepsilon_0\,\chi(\omega) \quad (4)$$

ε_r (Relative dielectric constant) and extinction coefficient κ are related with refractive index η as below

$$\eta + i\kappa = \sqrt{\varepsilon_r} \quad (5)$$

Where κ is the extinction coefficient, the dielectric constant is given as below in terms of the real (ε_1) and complex component (ε_2) is related with refractive index as below.

$$\eta = \sqrt{\frac{\sqrt{\varepsilon_1^2+\varepsilon_2^2}+\varepsilon_1}{2}} \quad \text{and} \quad k = \sqrt{\frac{\sqrt{\varepsilon_1^2+\varepsilon_2^2}-\varepsilon_1}{2}} \quad (6)$$

$$\varepsilon(\omega) = (\eta(\omega) + ik(\omega))^2 \quad (7)$$

The coefficient of optical absorption is correlated with the coefficient of extinction.

$$\alpha_\alpha = 2\frac{\omega}{c}\kappa \quad (8)$$

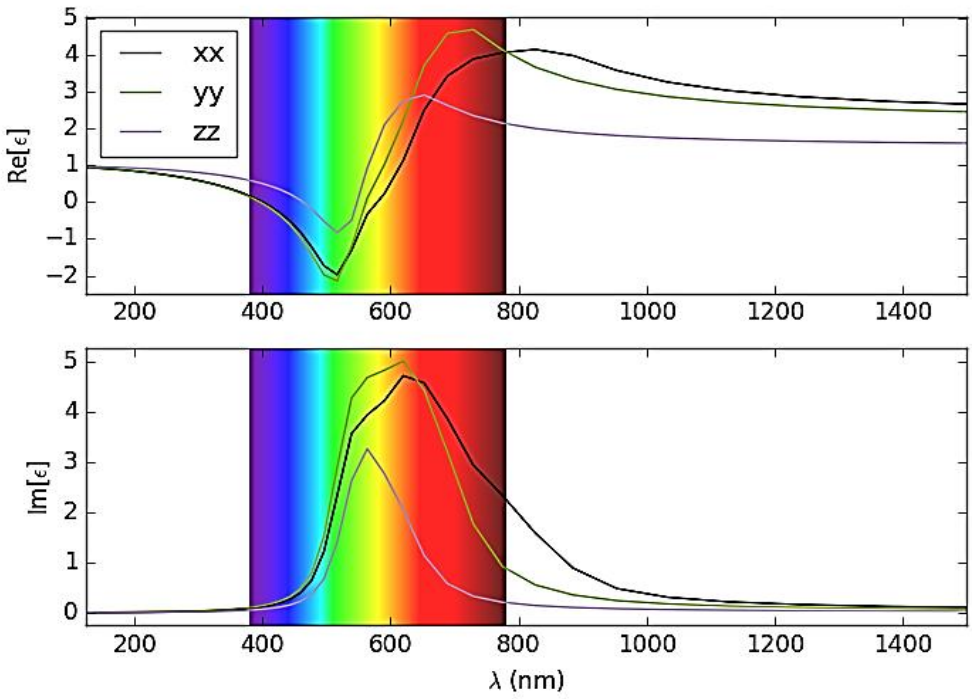

Fig. 4.18 Real (ε_1) and imaginary (ε_2) part of dielectric function (ε) v/s wavelength of MoS_2/ $Cd_{0.90}Zn_{0.10}Te_{0.93}Se_{0.07}$

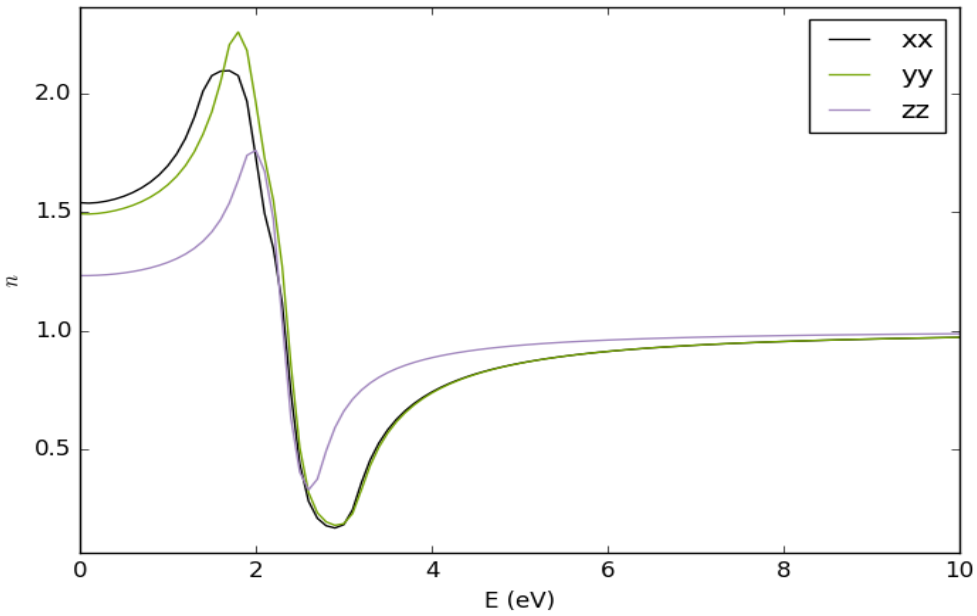

Fig. 4.19 Refractive index (η) v/s energy for $MoS_2/Cd_{0.90}Zn_{0.10}Te_{0.93}Se_{0.07}$

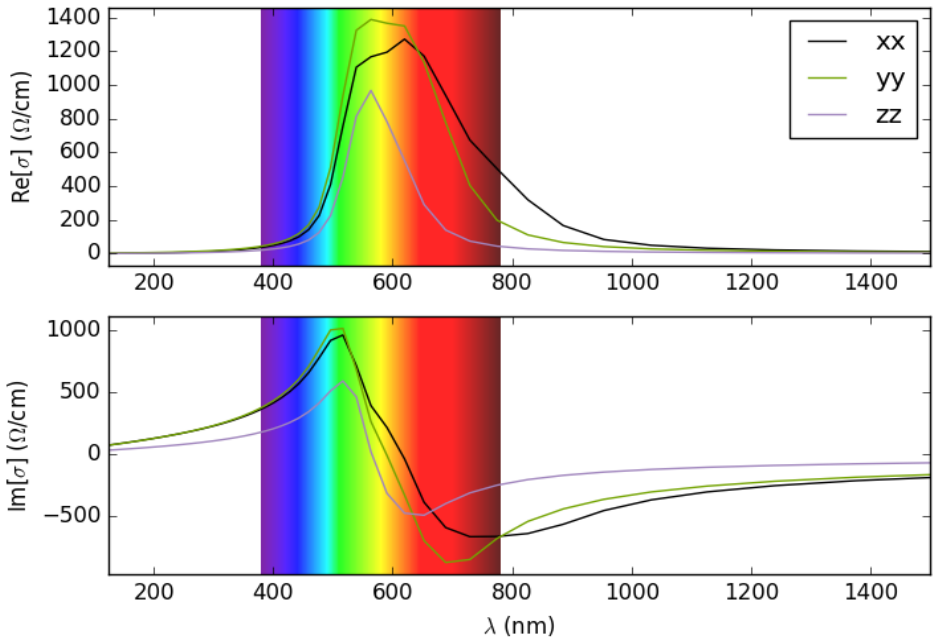

Fig. 4.20 Real and imaginary part of optical conductivity v/s wavelength of MoS_2/ $Cd_{0.90}Zn_{0.10}Te_{0.93}Se_{0.07}$

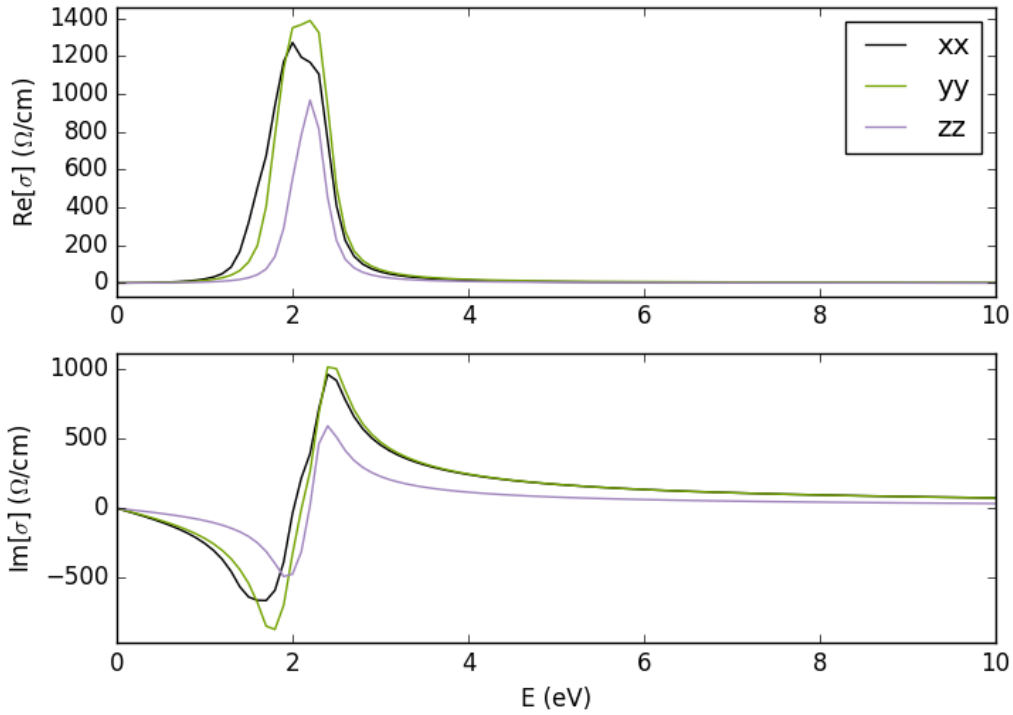

Fig. 4.21 Real and imaginary part of optical conductivity v/s energy of $MoS_2/Cd_{0.90}Zn_{0.10}Te_{0.93}Se_{0.07}$.

4.3 Analysis based on electronics properties

Density of states (DOS) and Energy band structure of individual material and heterostructure is represented above. Band structure and DOS and monolayer MoS_2 is shown in Figures 4.1 and 4.2 that is having direct band gap of 1.81eV and DOS also confirms the semiconducting nature that was also reported in [1] band gap in case of $Cd_{0.90}Zn_{0.10}Te_{0.93}Se_{0.07}$ was measured was 1.51 eV that is the confirmation work reported in [17] more interestingly in case of MoS_2 /$Cd_{0.90}Zn_{0.10}Te_{0.93}Se_{0.07}$ heterostructure reported direct bandgap was found to be 1.256 eV in Fig. 4.5 and DOS shows the semiconducting nature in Fig. 4.6

4.4 Analysis based on optical properties

In section 4.2, optical properties of $MoS_2/Cd_{0.90}Zn_{0.10}Te_{0.93}Se_{0.07}$ heterostructure and individual monolayers of MoS_2 and $Cd_{0.90}Zn_{0.10}Te_{0.93}Se_{0.07}$ are examined. The energy v/s dielectric function that includes both real and imaginary part describes the nature of the interaction of incident light when it will be propagating through the structure. The real part that describes the polarization effect and the imaginary part that describes the energy of the incident photons absorbed by the material Fig 4.18 shows the both real (ε_1) and imaginary

(ε_2) part of the dielectric function as function of photon energy along xx, yy, and zz tensors with peaks at ~2 eV that also consistent with the peaks of absorption coefficient in Fig.4.15 while in case of the other two material MoS_2 and $Cd_{0.90}Zn_{0.10}Te_{0.93}Se_{0.07}$ peaks are at much higher values as compared to heterostructure as in case of MoS_2 peak is at 3.8 eV and in case of $Cd_{0.90}Zn_{0.10}Te_{0.93}Se_{0.07}$ peaks can be seen between 3.8-5.8 eV. Hence shifting peaks of dielectric constant to the lower energy suggests that the excitonic binding energy of the system becomes smaller resulting in more absorption in visible spectrum and the system becomes more stable with an increase in efficiency. From Fig.4.7 and Fig.4.10 absorption coefficient v/s wavelength if we are going to compare the region of absorption in case of MoS_2 and $Cd_{0.90}Zn_{0.10}Te_{0.93}Se_{0.07}$ with Fig. 4.16 respectively it is clearly visible that the spectrum has been shifted towards lower energy levels the spectrum is completely bound in visible region that suggested that region of absorption is completely in visible region as compared to MoS_2 and $Cd_{0.90}Zn_{0.10}Te_{0.93}Se_{0.07}$.

Optical conductivity is also an important parameter that suggests the nature of the material towards the incident light energy and its electronic structure moreover it greatly depends on the absorption coefficient and frequency of light. But we cannot connect optical conductivity to the frequency and refractivity index in a single formula. Hence we are only considering the real part of optical conductivity that represents the light-matter interaction and measure of scattering of incident light hence in Fig.4.20 real part of optical conductivity shows the same trend as the absorption coefficient that shows the maximum conductivity at ~2 eV.

From Figure 4.9 absorption coefficient v/s wavelength if we are going to compare the region of absorption in the case of MoS_2 and $Cd_{0.90}Zn_{0.10}Te_{0.93}Se_{0.07}$ in Figures 3.9 and 3.13 respectively it is visible that the spectrum has been shifted towards lower energy levels the spectrum is completely bound in visible region that suggested that region of absorption is completely in the visible region as compared to MoS_2 and $Cd_{0.90}Zn_{0.10}Te_{0.93}Se_{0.07}$.

More if we are going to compare the both real (ε_1) and imaginary (ε_2) part of the dielectric function (ε) as a function of xx, yy, and zz tensors in the case of Figure 4.17 heterostructure all the two tensors xx and yy overlap while zz tensor is somehow separated which shows the isotropic nature of MoS_2 /$Cd_{0.90}Zn_{0.10}Te_{0.93}Se_{0.07}$ heterostructure which is also another advantage and can be used as polarizer material.

CHAPTER 5

CONCLUSIONS AND RECOMMENDATIONS

5.1 Conclusions

All the work that has been reported above employs the first principle DFT calculations to study the electronic and optical properties of $MoS_2/Cd_{0.90}Zn_{0.10}Te_{0.93}Se_{0.07}$ heterostructure. The heterostructure reported above resulted in very unique properties that resulted in a high value of absorption of incident radiation in the visible region of the spectrum while comparing with MoS_2 and $Cd_{0.90}Zn_{0.10}Te_{0.93}Se_{0.07}$ that were having absorption near-visible and UV region of the spectrum respectively.

$MoS_2/Cd_{0.90}Zn_{0.10}Te_{0.93}Se_{0.07}$ heterostructure is having all the absorption in the visible region with negligible contribution from UV and x-ray region in contrast to MoS_2 and $Cd_{0.90}Zn_{0.10}Te_{0.93}Se_{0.07}$. In optoelectronic application energy conversion devices like photodetectors, solar cells use the visible spectrum that incident photons must be having enough energy to knock out the electrons or creation of electron-hole pair that would be sufficient in creating an electric current. As we have seen that the major contribution in the case of both MoS_2 and $Cd_{0.90}Zn_{0.10}Te_{0.93}Se_{0.07}$ from x rays and UV region that is of no use for optoelectronics application absorption in these regions is directly proportional to more heating of the device and also reduces the efficiency so it is a clear observation that the devices fabricated with only MoS_2 and $Cd_{0.90}Zn_{0.10}Te_{0.93}Se_{0.07}$ will be having more heating problem with reduced efficiency than devices fabricated with their heterostructure hence because of its complete absorption in the visible region makes this heterostructure revolutionary material in optoelectronics applications.

5.2 RECOMMENDATIONS

DFT based calculations performed on $MoS_2/Cd_{0.90}Zn_{0.10}Te_{0.93}Se_{0.07}$ heterostructure and its individual constituent material. We discussed how the band gap can be changed by manipulating the structure as we saw in case of MoS_2. Resulted heterostructure shows the remarkable absorption in visible region of electromagnetic spectrum hence this heterostructure claims itself a dominant material for optoelectronics applications in the field of telecommunication, fabrications of solar cells, displays, phototransistors and photodiode.

REFERENCES

[1] K. F. Mak, C. Lee, J. Hone, J. Shan, and T. F. Heinz, “Atomically thin MoS2: A new direct-gap semiconductor,” Phys. Rev. Lett., vol. 105, 2010, Art. no. 136805.

[2] W. Zhang, J. K. Huang, C. H. Chen, Y. H. Chang, Y. J. Cheng, and L. J. Li, “High-gain phototransistors based on a CVD MoS2 monolayer,” Adv. Mater., vol. 25, no. 25, pp. 3456–3461, 2013.

[3] A. K. Geim and K. S. Novoselov, “The rise of graphene,” Nature Mater., vol. 6, pp. 183–189, 2007.

[4] X. Duan, C. Wang, A. Pan, R. Yu, and X. Duan, “Two-dimensional transition metal dichalcogenides as atomically thin semiconductors: Opportunities and challenge,” *Chem. Soc. Rev.*, vol. 44, pp. 8859–8876, 2015.

[5] K. S. Novoselov, A. Mishchenko, A. Carvalho, A. C. Neto, "2D materials and van der Waals heterostructures", *Science*, vol. 353, no. 6298, 2016.

[6]H. Liu et al., “Phosphorene: An unexplored 2D semiconductor with a high hole mobility,” ACS Nano, vol. 8, no. 4, pp. 4033–4041, 2014.

[7] R. Kochar and S. Choudhary,“MoS2/phosphorene heterostructure for optical absorption in visible region,” IEEE J. Quantum Electron., vol. 54, no. 4, 2018, Art no. 7000306.

[8] Yu, L. et al. Graphene/MoS2 hybrid technology for large-scale two-dimensional electronics. Nano Lett. 14, 3055–3063 (2014).

[9] Splendiani, A. et al. “Emerging photoluminescence in monolayer MoS_2. Nano Lett. 10, 1271–91275 (2010)

[10] H J.Monkhorst and J. D. Pack, “Special points for brillouin-zone integrations, Phys. Rev. B, vol. 13, 1976, Art. no. 5188.

[11] Li, L. et al. “Raman shift and electrical properties of MoS2 bilayer on boron nitride substrate. Nanotechnology” 26, 295702 (2015).

[12] Yu, Y. et al. “Engineering substrate interactions for high luminescence efficiency of transition-metal dichalcogenides monolayers”. Adv. Funct. Mater. 26, 4733–4739 (2016)

[13] Bolotnikov, A. E. et al. “Te Inclusions in CZT Detectors: New Method for Correcting Their Adverse Effects”. IEEE Trans. on Nucl. Sc. 57, 910 (2010).

[14] Roy, U.N., Camarda, G.S., Cui, Y. et al. “Role of selenium addition to CdZnTe matrix for room-temperature radiation detector applications”. Sci Rep 9, 1620 (2019)

[15] Yuan Liu1, Nathan O. Weiss1, Xidong Duan2, Hung-Chieh Cheng, Yu Huang

and Xiang feng Duan. “Van der Waals heterostructures and devices” Nature mater. vol. 1, no. 2016, Art. no. 16042.

[16] Ming-Yang Li, Chang-Hsiao Chen, Yumeng Shi and Lain-Jong, “Heterostructures based on two-dimensional layered materials and their potential applications” Materials Today Vol. 00, No 00, December 2015, pp. 1369-7021

[17] Utpal N. Roy, Giuseppe S. Camarda1, Yonggang Cui1, Rubi Gul1, Ge Yang, Jakub Zazvorka, Vaclav Dedic, Jan Franc & Ralph B. James “Evaluation of CdZnTeSe as a high quality gamma-ray spectroscopic material with better compositional homogeneity and reduced defects” Sci Rep 9, 1620 (2018)

[18] A. K. Geim & I. V. Grigorieva1 “Van der Waals heterostructures” Nature mater. vol. 8, Art no. 12385

[19] Tadayuki Takahashi and Shin Watanabe, “Recent Progress in CdTe and CdZnTe Detectors”IEEE Trans. Nucl. Sci, Vol. 48, AUG 2001

[20] Sudhanshu Choudhary and Achal Kumar Garg, “Enhanced Absorption in MoS2/Hg0.33Cd0.66Te Heterostructure for Application in Solar Cell Absorbers” IEEE Trans. on Nanotech,Vol. 18, 2019

[21] Kin Fai Mak and Jie Shan “Photonics and optoelectronics of 2D semiconductor transition metal dichalcogenides” Nature photonics Vol. 10, 2016

[22] Adriana Pecoraro, Eduardo Schiavo Pasqualino Maddalena2 Ana B. Muñoz-García2, Michele Pavone “Structural and electronic properties of defective 2D transition metal dichalcogenide heterostructures” J Comput Chem. 2020; 1–10

[23] Xiao Li , Hongwei Zhu “Two-dimensional MoS2: Properties, preparation, and applications” ScienceDirect , J. Mater. mics,1 2015; 33-44.

[24] G. Kresse and J. Furthmüller, “Efficient iterative schemes for ab initio total energy calculations using a plane-wave basis set,” Phys. Rev. B, vol. 54, 1996, Art. no. 11169.

[25] J. P. Perdew, K. Burke, and M. Ernzerhof, “Generalized gradient approximation made simple,” Phys. Rev. Lett., vol. 77, pp. 3865–3868, 1996.

[26] H J.Monkhorst and J. D. Pack, “Special points for brillouin-zone integrations, Phys. Rev. B, vol. 13, 1976, Art. no. 5188.

[27] Dechao Geng and Hui Ying Yang “Recent Advances in Growth of Novel 2D Materials: Beyond Graphene and Transition Metal Dichalcogenides” Adv. Mater. 2018, 1800865.

[28] Stefano Del Sordo , Leonardo Abbene, Ezio Caroli , Anna Maria Mancini , Andrea Zappettini and Pietro Ubertini “Progress in the Development of CdTe and CdZnTe Semiconductor Radiation Detectors for Astrophysical and Medical Applications” *Sensors* 2009, *9*, 3491-3526.